MITSUBISHI ELECTRIC RESEARCH LABORATORIES
http://www.merl.com

QoS-Constrained Relay Control for Full-Duplex Relaying with SWIPT

Liu, H.; Kim, K.J.; Kwak, K.S.; Poor, H.V.

TR2017-105 March 2017

Abstract

This study investigates relay control for simultaneous wireless information and power transfer in full-duplex relay networks under Nakagami-m fading channels. Unlike previous work, harvest-transmit (HT) and general harvest-transmit-store (HTS) models are respectively considered to maximize average throughput subject to quality of service (QoS) constraints. The end-to-end outage probability of the network in an HT model is presented in an exact integral-form. To prevent outage performance degradation in an HT model, time switching (TS) is designed to maximize average throughput subject to QoS constraints of minimizing outage probability and maintaining a target outage probability, respectively. The optimal TS factors subject to QoS constraints are presented for an HT model. In general, in an HTS model, energy scheduling is performed across different transmission blocks and TS is performed within each block. Compared with the block-based HTS model without TS, the proposed general HTS model can greatly improve outage performance via greedy search (GS). By modeling the relay's energy levels as a Markov chain with a two-stage state transition, the outage probability for GS implementation of the general HTS model is derived. To demonstrate the practical significance of QoS-constrained relay control, numerical results are presented showing that the proposed relay control achieves substantial improvement of outage performance and successful rate.

IEEE Transactions on Wireless Communications

QoS-Constrained Relay Control for Full-Duplex Relaying with SWIPT

Hongwu Liu, *Member, IEEE,* Kyeong Jin Kim, *Senior Member, IEEE,*
Kyung Sup Kwak, *Member, IEEE,* and H. Vincent Poor, *Fellow, IEEE*

***Abstract*—This study investigates relay control for simultaneous wireless information and power transfer in full-duplex relay networks under Nakagami-m fading channels. Unlike previous work, harvest-transmit (HT) and general harvest-transmit-store (HTS) models are respectively considered to maximize average throughput subject to quality of service (QoS) constraints. The end-to-end outage probability of the network in an HT model is presented in an exact integral-form. To prevent outage performance degradation in an HT model, time switching (TS) is designed to maximize average throughput subject to QoS constraints of minimizing outage probability and maintaining a target outage probability, respectively. The optimal TS factors subject to QoS constraints are presented for an HT model. In general, in an HTS model, energy scheduling is performed across different transmission blocks and TS is performed within each block. Compared with the block-based HTS model without TS, the proposed general HTS model can greatly improve outage performance via greedy search (GS). By modeling the relay's energy levels as a Markov chain with a two-stage state transition, the outage probability for GS implementation of the general HTS model is derived. To demonstrate the practical significance of QoS-constrained relay control, numerical results are presented showing that the proposed relay control achieves substantial improvement of outage performance and successful rate.**

***Index Terms*—Energy harvesting, wireless power transfer, amplify-and-forward relay, full-duplex relay, relay control.**

I. Introduction

With capability to harvest energy from ambient radio-frequency (RF) signals, simultaneous wireless information and power transfer (SWIPT) techniques provide a more promising way for wireless communications to function in environments with physical or other limitations [1]–[3]. Based on two practical receiver architectures, namely, time switching (TS) and power splitting (PS) receivers [1], SWIPT techniques have been widely applied in wireless networks [3, and references therein]. One line of research that has emerged is relay-assisted SWIPT [4]–[11]. It has shown that relay-assisted SWIPT not only enables wireless communications over long distances or across barriers, but also keeps energy-constrained relays active through RF energy harvesting (EH). In [4] and [5], TS and PS relaying protocols have been designed for amplify-and-forward (AF) and decode-and-forward (DF) relay networks, respectively. Several power allocation schemes for relay-assisted SWIPT networks with multiple source-destination pairs were studied in [6]. Outage probability and diversity of relay-assisted SWIPT networks with spatial randomly located relays were investigated in [10] and distributed PS-based SWIPT was investigated for interference relay networks in [11]. Moreover, multi-antenna technologies have been applied in relay-assisted SWIPT networks in [7]–[9]. Nevertheless, all these studies are limited to half-duplex relay (HDR) mode. Since the source-to-relay and relay-to-destination channels are kept orthogonal by either frequency division or time division multiplexing, about 50% spectral efficiency (SE) loss occurs in HDR mode. As a key technology for future relay networks, full-duplex relay (FDR) systems have drawn considerable attention [12]–[18]. Since FDR mode realizes an end-to-end (e2e) transmission via one channel utilization, significant improvement of SE over HDR mode can be achieved.

A few studies have been conducted for FDR-assisted SWIPT networks. In [14] and [15], outage probability, throughput, and ergodic capacity have been analyzed for FDR-assisted SWIPT networks, in which a TS-based relay is operated cooperatively. In practice, since an FDR node suffers severe self-interference from its own transmit signal, FDR transmission is difficult to implement. To suppress self-interference, MIMO antennas have been employed at the relay to aid FDR-assisted SWIPT [19]. For conventional two-phase AF HDR networks, a self-interference immunized FDR node was proposed by employing EH in the second time phase [20], so that the relay can transmit information and extract energy simultaneously via separated transmit and receive antennas. Note that all the above studies of FDR-assisted SWIPT are conducted to maximize network throughput without further considering quality of service (QoS) constraints, whereas it is envisioned that SWIPT techniques will be required to support various types of traffic having different QoS requirements [21]–[23]. For point-to-multipoint PS-based SWIPT networks, QoS constraints based on signal-to-interference-plus-noise ra-

Manuscript received December 29, 2015; revised June 21, 2016 and October 18, 2016; accepted February 8, 2017. This work was supported in part by SRF for ROCS, SEM, Shandong Provincial Natural Science Foundation, China, under Grant 2014ZRB019XM, in part by the Ministry of Science, ICT and Future Planning (MSIP), Korea, under the Information Technology Research Center Support Program supervised by the Institute for Information and Communications Technology Promotion under Grant IITP-2016-H8501-16-1019, in part by the National Research Foundation of Korea, Grant Funded by the Korean Government, MSIP, under Grant NRF-2017R1A2B2012337, and in part by the U.S. National Science Foundation under Grant ECCS-1343210. The associate editor coordinating the review of this paper and approving it for publication was Y. Jing. *(Corresponding author: Kyung Sup Kwak.)*

H. Liu is with Shandong Jiaotong University, Jinan 250357, China (e-mail: hong.w.liu@hotmail.com).

K. J. Kim is with Mitsubishi Electric Research Laboratories, Cambridge, MA 02139 USA (e-mail: kyeong.j.kim@hotmail.com).

K. S. Kwak (corresponding author) is with the Department of Information and Communication Engineering, Inha University, Incheon 22212, South Korea (e-mail: kskwak@inha.ac.kr).

H. V. Poor is with the Department of Electrical Engineering, Princeton University, Princeton, NJ 08544 USA (e-mail: poor@princeton.edu).

tio (SINR) and mean-square-error (MSE) have been applied to minimize transmission power in [21] and [24], respectively. A game-theoretic approach has been applied to optimize multiple-pair SWIPT communications subject to SINR and EH constraints in [25]. For TS-based SWIPT, [23] studies joint TS and power control to maintain a given level of throughput. Notably, all the above control schemes are based on estimation of instantaneous channel state information (CSI), which requires dedicated reverse-link training from the EH receiver [26].

Motivated by these previous studies, in this paper we consider the maximization of average throughput for a QoS-constrained FDR network with SWIPT. In the considered FDR network, the source has a reliable power supply, whereas the relay has to harvest energy from the source-emitted RF signal via TS operation[1]. Since TS affects both SE and QoS, the relaying mode and corresponding TS have a complicated relationship in achieving the allowable maximum SE subject to QoS constraints. Compared with existing works, some distinct features of our study are highlighted here.

- In [20], the effective information transmission time is the same as that of HDR networks, so that the SE improvement is achieved in HDR mode rather than FDR mode. In our study, we consider maximization of average throughput of FDR transmission, i.e., the relay receives and forwards the source information to the destination simultaneously.
- Zhong *et al*. [14] and [15] investigated FDR-assisted SWIPT in the harvest-transmit (HT) model to improve average throughput with optimized TS. Unfortunately, outage performance seriously degrades in delay-limited transmissions when TS is optimized without a QoS constraint. In our study, both outage probability minimization and target outage probability are adopted as QoS constraints, under which TS is optimized to achieve the allowable maximum average throughput. Thus, serious outage performance degradation can be prevented and successful rate can be maximized [27].
- The analysis of outage probability and throughput in [14] and [15] are conducted by modeling dual-hop and residual self-interference (RSI) channels as Rayleigh fading. However, SWIPT operates most efficiently within a relatively short range. In this situation, a line of sight (LoS) path exists with high probability and Nakagami-m fading can provides a better model [9], [28]. Furthermore, although a Rician fading model is appropriate for the RSI channel in the RF-domain [29], the exact behavior of the RSI channel in the digital-domain is still unknown due to several complicated stages of active interference cancellation (IC) [30], [31]. Therefore, this study investigates outage probability conditioned on the RSI channel power without modeling the RSI channel gain via a specific distribution and considers Nakagami-m fading for dual-hop channels, so that our analytical results can be applied to a wide range of FDR-assisted SWIPT networks employing different IC schemes.
- Due to propagation loss and channel fluctuations, the relay-harvested energy within a transmission block can be very limited and energy accumulation is needed to improve the reliability of information transmission [32], [33]. Different from the block-based harvest-transmit-store (HTS) model [32], this study considers a general HTS model by employing TS within each transmission block. With the aid of in-block TS, the general HTS model can greatly improve outage performance and includes the block-based HTS model as a special case.

In this paper, the HT model and the general HTS are investigated subject to QoS constraints. The corresponding control schemes are developed and analytical results are presented to verify the QoS metrics. The contributions of the paper are summarized as follows:

- By modeling dual-hop channels as Nakagami-m fading, we present the analytical e2e outage probability conditioned on the RSI channel power for the HT model. QoS constraints of minimizing outage probability and maintaining a target outage probability are respectively considered in optimizing TS to achieve the allowable maximum average throughput. The optimal TS factor that maximizes average throughput subject to minimizing outage probability is presented in closed form. The optimal TS factor that maximizes average throughput subject to a target outage probability is also derived. Employing the obtained optimal TS factors, the successful rate is achieved with the guaranteed outage performance.
- To accumulate energy for optimizing FDR transmission, a general HTS model is designed by employing TS within each block. In the general HTS model, the first phase of each block is dedicated for EH. In the second phase of each block, the relay node can switch to EH or FDR transmission depending on the relay's residual energy level and CSI. A greedy search (GS) policy is implemented to realize the proposed general HTS model. By allocating a small portion of time for EH within each block, the GS policy improves outage performance significantly over that of the block-based HTS model [32].
- The proposed general HTS model degenerates to the block-based HTS model by setting a zero TS factor. Thus, the general HTS model and the block-based HTS model can be analyzed under a uniform framework. With respect to the time-switched two operational phases in each block, the relay's residual energy levels are modeled as a Markov chain (MC) with a two-stage state transition. Then, the e2e outage probability is derived for the GS implementation of the general HTS mode including the block-based HTS model as a special case.

The rest of this paper is organized as follows. Section II describes the HT model and develops its e2e outage probability. The optimal TS that maximizes average throughput subject to QoS constraints is also derived in Section II. Section III

[1] This setting has a number of potential applications in energy-limited wireless networks, e.g., when the intermediate node is energy-selfish or lacks an energy-supply, or the direct link from the source to destination is blocked by a barrier while the relay has to be placed on a site without a fixed power supply.

presents the general HTS model and its GS implementation. The analytical e2e outage probability for the GS policy is also derived in Section III. Section IV presents numerical results and discusses the system performances of the proposed control schemes. Finally, Section V summarizes the contributions of our study.

Notation: $\lfloor \cdot \rfloor$ is the floor function, $F_X(\cdot)$ and $\bar{F}_X(\cdot)$ denote the cumulative distribution function (CDF) and the complementary CDF (CCDF) of the random variable X, respectively, $\Gamma(\cdot)$ denotes the gamma function, $\Gamma_u(\cdot,\cdot)$ denotes the upper incomplete gamma function, and $K_n(\cdot)$ is the n-th order modified Bessel function of the second kind [34, Eq. 8.432].

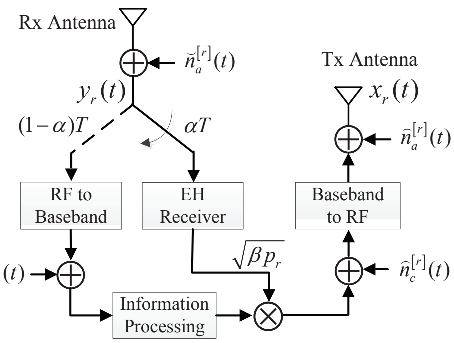

Fig. 1. Block diagram of the considered FDR node.

II. Harvest-Transmit Model

In this paper, we consider a wireless dual-hop FDR network, in which a source node intends to transfer its information to the destination node. Due to physical isolation or environmental limitations between the source and destination, a cooperative relay is employed to assist information transmission from the source to the destination. The relay is assumed to be an energy-selfish or energy-constrained device such that it needs to harvest energy from the source-emitted RF signal to forward the source information to the destination. For simplicity of implementation, the AF relaying scheme and TS architecture are chosen at the relay. The channels of the source-to-relay and relay-to-destination links are denoted by $h_1 = \sqrt{\mathcal{L}_1}\tilde{h}_1$ and $h_2 = \sqrt{\mathcal{L}_2}\tilde{h}_2$, respectively, where $\mathcal{L}_i$ and $\tilde{h}_i$ $(i = 1, 2)$ are large-scale fading and small-scale fading of the dual-hop channels, respectively. The large-scale fading is comprised of the distance-dependent path loss as well as shadowing attenuation, i.e.,

$$\mathcal{L}_i \triangleq \frac{\mathcal{A}_i \mathcal{L}_0 \mathcal{L}_s}{(d_i/d_0)^{\varphi}}, \tag{1}$$

where $\mathcal{A}_i$ is the transmit antenna gain of the i-th hop link, $\mathcal{L}_0$ is the measured path loss at the reference distance d_0, d_i is the distance between the transmitter and receiver of the i-th hop link, φ is the path loss exponent, and $\mathcal{L}_s$ is the shadowing attenuation. To account for the LoS communication setting, the shadowing attenuation is set to $\mathcal{L}_s = 1$ in this study. For the sake of exposition, the channel gain of h_i is denoted by $g_i \triangleq |h_i|^2$ for $i \in \{1, 2\}$. The small-scale channel magnitude of the dual-hop links, $|\tilde{h}_i|$, is modeled as Nakagami-m fading with unit mean such that g_i is distributed according to the gamma distribution with shape factor m_i and scale factor $\theta_i \triangleq \frac{\bar{g}_i}{m_i}$, where $\bar{g}_i \triangleq \mathbb{E}\{|h_i|^2\}$ is the average channel gain for $i \in \{1, 2\}$. Then, the CDF and CCDF of g_i $(i = 1, 2)$ can be respectively expressed as

$$F_{g_i}(x) = 1 - \frac{\Gamma_u(m_i, x/\theta_i)}{\Gamma(m_i)} \text{ and } \bar{F}_{g_i}(x) = \frac{\Gamma_u(m_i, x/\theta_i)}{\Gamma(m_i)}. \tag{2}$$

For energy-constrained networks, the CSI can be estimated via dedicated reverse-link training from the EH receiver by employing a two-phase training-transmission protocol [26] and hence, we assume that the relay can access perfect dual-hop CSI in this study.

According to the experimental results of [29], the RSI channel incident on the receive antenna at a full-duplex node can be characterized as Rician. Nevertheless, RSI cannot be eliminated completely because of RF impairments [35] and the e2e detection performance of FDR networks is still limited by RSI [36]. To the best of our knowledge, after several complicated stages of active IC, the distribution of the RSI observed in the digital-domain is not known in practice [30], [31], [36]. In this study, the RSI channel and RSI channel power in the digital-domain after active IC are denoted by h_r and $g_r \triangleq |h_r|^2$, respectively. Furthermore, the normalized transmitted signals of the source and relay are denoted by $x_s(t)$ and $x_r(t)$, respectively, and the transmission powers at the source and relay are denoted by p_s and p_r, respectively.

In the HT model, each transmission block with a duration of T is divided into two phases for EH and FDR transmission, respectively. Denoting the TS factor by α $(0 < \alpha < 1)$, the first phase assigned with a duration of αT is applied for power transfer from the source to the relay. The second phase assigned with the remaining duration of $(1-\alpha)T$ is used for FDR transmission. The relay-received RF signals in the two phases are sent to the EH receiver and information processing (IP) receiver, respectively, as illustrated in Fig. 1. With respect to the EH receivers's sensitivity $S_{\min}$ [37], a piecewise behavior is assumed in the HT model, i.e., the EH and IP receivers at the relay are activated only when

$$p_s g_1 \geq S_{\min}, \tag{3}$$

otherwise the EH and IP receivers keep silent. When (3) is satisfied, the harvested energy at the relay can be expressed as

$$E_h = \eta_h p_s g_1 \alpha T, \tag{4}$$

where η_h is the energy conversion efficiency depending on the rectifier circuit [37]. By utilizing the harvested energy in the first phase, the relay transmission power in the second phase is given by

$$p_r = \frac{\eta_t E_h}{(1-\alpha)T} \triangleq \kappa p_s g_1, \tag{5}$$

where $\eta_t \in (0, 1)$ is the energy utilization efficiency and $\kappa \triangleq \frac{\alpha\eta_h\eta_t}{1-\alpha}$. For the sake of exposition, we assume a normalized block duration in the sequel and hence, we can use the terms power and energy interchangeably.

In the FDR mode, the relay concurrently receives the signal $y_r(t)$ and transmits the signal $x_r(t)$ on the same frequency, as depicted in Fig. 1, where $\breve{n}_a^{[r]}(t)$ and $\widehat{n}_a^{[r]}(t)$ are narrow-band Gaussian noises introduced by the receive and transmit antennas, respectively. In addition, $\breve{n}_c^{[r]}(t)$ and $\widehat{n}_c^{[r]}(t)$ are baseband additive white Gaussian noises (AWGNs) caused by down-conversion and up-conversion, respectively [1]. For simplicity, the equivalent baseband noise comprising both $\breve{n}_a^{[r]}(t)$ and $\widehat{n}_a^{[r]}(t)$ is modeled by the zero mean AWGN $n_a^{[r]}(t)$ with variance σ_a^2, and the equivalent baseband noise comprising both $\breve{n}_c^{[r]}(t)$ and $\widehat{n}_c^{[r]}(t)$ is modeled by the zero mean AWGN $n_c^{[r]}(t)$ with variance σ_c^2. Then, the overall AWGN at the relay can be modeled as the zero mean AWGN $n_r(k) \triangleq n_a^{[r]}(k) + n_c^{[r]}(k)$ with variance $\sigma_r^2 \triangleq \sigma_a^2 + \sigma_c^2$. The sampled baseband signal after some stages of IC is given by

$$y_r(k) = \sqrt{p_s} h_1 x_s(k) + h_r x_r(k) + n_r(k), \tag{6}$$

where k denotes the symbol index, $x_s(k)$ and $x_r(k)$ are the sampled signals of $x_s(t)$ and $x_r(t)$, respectively. The transmitted signal in (6) can be expressed as

$$x_r(k) = \sqrt{\beta} y_r(k - \tau), \tag{7}$$

where $\tau \geq 1$ is the processing delay at the relay and $\beta = (p_s g_1 + p_r g_r + \sigma_r^2)^{-1}$ is the normalization coefficient. The sampled received signal at the destination is given by

$$y_d(k) = \sqrt{p_r} h_2 x_r(k) + n_d(k), \tag{8}$$

where $n_d(k)$ is the additive noise at the destination with zero mean and variance σ_d^2. In this network, the e2e SINR can be expressed as

$$\gamma_{\mathrm{e2e}} = \frac{\gamma_{\mathrm{R}} \gamma_{\mathrm{D}}}{\gamma_{\mathrm{R}} + \gamma_{\mathrm{D}} + 1}, \tag{9}$$

where $\gamma_{\mathrm{R}} \triangleq \frac{p_s g_1}{p_r g_r + \sigma_r^2}$ and $\gamma_{\mathrm{D}} \triangleq \frac{p_r g_2}{\sigma_d^2}$ are the SINRs at the relay and destination, respectively.

In each transmission block, an outage event occurs when the power of the ambient RF signal at the relay is less than the EH receiver sensitivity or when the e2e SINR is less than the required threshold for correct data detection given that EH is successful. Therefore, the e2e outage probability in the HT model can be expressed as

$$\begin{aligned} P_{\mathrm{out}} \triangleq\ & \Pr\{p_s g_1 < S_{\min}\} \\ & + \Pr\{(p_s g_1 \geq S_{\min}) \cap (\gamma_{\mathrm{e2e}} < \gamma_{\mathrm{th}})\}, \end{aligned} \tag{10}$$

where γ_{th} is the e2e SINR threshold for correct data detection at the destination. Note that in conventional AF relay networks without EH, the information outage probability is defined as

$$P_{\mathrm{out}}^{\mathrm{I}} \triangleq \Pr\{\gamma_{\mathrm{e2e}} < \gamma_{\mathrm{th}}\}. \tag{11}$$

Then, the average throughput can be expressed as

$$R_{\mathrm{HT}} = (1-\alpha)(1 - P_{\mathrm{out}}) R, \tag{12}$$

where $R \triangleq \log_2(1 + \gamma_{\mathrm{th}})$ is the fixed transmission rate. The design goal is to maximize the average throughput by optimizing TS subject to QoS constraints. The optimal α^* can be obtained by solving the following maximization problem:

$$\alpha^* = \arg\max_{\alpha} R_{\mathrm{HT}}(\alpha), \quad \text{s.t. } 0 < \alpha < 1 \text{ and } Q_i, \tag{13}$$

where $Q_i \in \{Q_1, Q_2\}$ is a QoS constraint as we will explain later. Notably, without considering a QoS constraint, the achievable maximum average throughput of (13) may be obtained by a large $1-\alpha$ at the cost of a large $P_{\mathrm{out}}^{\mathrm{I}}$, which greatly degrades the system performance due to a large amount of repetition transmissions [27], [38]. Therefore, the QoS requirements of decreasing outage probability [38] and maintaining a target outage probability [27] are respectively considered, i.e.,

$$Q_1 := \{P_{\mathrm{out}}^{\mathrm{I}} \text{ is minimized}\} \quad \text{and} \quad Q_2 := \{P_{\mathrm{out}}^{\mathrm{I}} \leq \varepsilon\}, \tag{14}$$

where ε is a given target information outage probability [27]. To obtain α^*, the immediate task is to characterize the e2e outage probability of the system. For the sake of mathematical tractability, we focus on the RSI dominated scenario which is of practical interest [12], [14].

Proposition 1. *Conditioned on g_r, the e2e outage probability of the system in the HT model is given by*

$$P_{\mathrm{out}} = 1 - (1 - P_{\mathrm{out}}^{\mathrm{I}}) \bar{F}_{g_1}\left(\frac{S_{\min}}{p_s}\right), \tag{15}$$

where

$$P_{\mathrm{out}}^{\mathrm{I}} = \begin{cases} \frac{2^{2-m_1-m_2}}{\Gamma(m_1)\Gamma(m_2)} D_{\mu,\nu}(2\sqrt{\xi}), & 0 < \alpha < \frac{1}{1+\eta g_r \gamma_{\mathrm{th}}} \\ 1, & \frac{1}{1+\eta g_r \gamma_{\mathrm{th}}} \leq \alpha < 1 \end{cases}, \tag{16}$$

$$\xi \triangleq \frac{\gamma_{\mathrm{th}} \sigma_d^2 (1 + \kappa g_r)}{\kappa p_s \theta_1 \theta_2 (1 - \kappa \gamma_{\mathrm{th}} g_r)}, \tag{17}$$

$\mu = m_1 + m_2 - 1$, $\nu = m_1 - m_2$, $D_{\mu,\nu}(y) = \int_0^y x^\mu K_\nu(x) \mathrm{d}x$, *and* $\bar{F}_{g_1}(x) \triangleq \frac{\Gamma_u(m_1, x/\theta_1)}{\Gamma(m_1)}$ *is the CCDF of* g_1.

Proof. See Appendix A. □

Proposition 1 shows that when $\frac{1}{1+\eta g_r \gamma_{\mathrm{th}}} \leq \alpha < 1$, $P_{\mathrm{out}} = 1$. To avoid $P_{\mathrm{out}} = 1$, it is required to set $0 < \alpha < \frac{1}{1+\eta g_r \gamma_{\mathrm{th}}}$ or equivalently to eliminate the RSI by $g_r < \frac{1}{\kappa \gamma_{\mathrm{th}}}$. Moreover, as $p_s \to \infty$, we have $\bar{F}_{g_1}\left(\frac{S_{\min}}{p_s}\right) \to 1$ and

$$P_{\mathrm{out}} = P_{\mathrm{out}}^{\mathrm{I}} \to \begin{cases} 0, & 0 < \alpha < \frac{1}{1+\eta g_r \gamma_{\mathrm{th}}} \\ 1, & \frac{1}{1+\eta g_r \gamma_{\mathrm{th}}} \leq \alpha < 1 \end{cases}. \tag{18}$$

Thus, $P_{\mathrm{out}}^{\mathrm{I}} \to 0$ and $P_{\mathrm{out}} \to 0$ can be achieved by setting $\alpha \in (0, \frac{1}{1+\eta g_r \gamma_{\mathrm{th}}})$ as $p_s \to \infty$. Furthermore, as $p_s \to \infty$ and $g_r \to 0$, we can achieve $P_{\mathrm{out}}^{\mathrm{I}} \to 0$ and $P_{\mathrm{out}} \to 0$ by setting $\alpha \in (0, 1)$. Recalling that the effective FDR transmission time is $1 - \alpha$, α should be set as small as possible to achieve the allowable maximum average throughput. Thus, it can be shown that the optimal solution of (13) with the QoS constraint Q_1 is $\alpha^* \to 0$ as $p_s \to \infty$.

With the obtained $P_{\mathrm{out}}^{\mathrm{I}}$ of (16), maximizing $1 - P_{\mathrm{out}}$ is equivalent to maximizing $1 - P_{\mathrm{out}}^{\mathrm{I}}$. Then, the maximization problem (13) can be simplified as

$$\alpha^* = \arg\max_{\alpha} \ (1-\alpha)(1 - P_{\mathrm{out}}^{\mathrm{I}}), \tag{19a}$$

$$\text{s.t.} \ \ 0 < \alpha < \frac{1}{1 + \eta g_r \gamma_{\mathrm{th}}} \text{ and } Q_i. \tag{19b}$$

Since outage probability and successful rate are two important metrics in delay-limited transmissions [27], [39], we also consider the successful rate for the FDR-assisted SWIPT network. According to [27], the successful rate is defined as the product of the fixed transmission rate and the success probability. With respect to TS operation, we define the successful rate for the considered FDR-assisted SWIPT network as

$$R_{\mathrm{HT}}^{(\mathrm{s})} \triangleq \begin{cases} (1-\alpha)(1-\varepsilon)R, & P_{\mathrm{out}} \le \varepsilon \\ 0, & \mathrm{otherwise}, \end{cases} \tag{20}$$

where we have assumed that the physical-layer outage is fixed to the target outage probability [27]. Obviously, the successful rate is a strictly QoS-dependent metric, which represents the average throughput subject to an explicitly defined outage constraint. To achieve a non-zero successful rate, the obtained $P_{\mathrm{out}}^{\mathrm{I}}$ subject to the outage constraint should be less than or equal to ε when $p_s g_1 \ge S_{\min}$. In the following, the optimal TS factors of (19) subject to Q_1 and Q_2 are respectively presented.

Proposition 2. *The optimal TS factor that maximizes the average throughput subject to Q_1 in the HT model is given by*

$$\bar{\alpha} = \frac{1}{1+\eta g_r(\sqrt{\gamma_{\mathrm{th}}(\gamma_{\mathrm{th}}+1)}+\gamma_{\mathrm{th}})} \tag{21}$$

and the corresponding information outage probability is given by

$$\bar{P}_{\mathrm{out}}^{\mathrm{I}} = \tfrac{2^{2-m_1-m_2}}{\Gamma(m_1)\Gamma(m_2)} D_{\mu,\nu}\left(2\sqrt{\bar{\xi}}\right), \tag{22}$$

where

$$\bar{\xi} \triangleq \frac{g_r\gamma_{\mathrm{th}}\sigma_d^2\left(2\left(\gamma_{\mathrm{th}}+\sqrt{\gamma_{\mathrm{th}}(\gamma_{\mathrm{th}}+1)}\right)+1\right)}{p_s\theta_1\theta_2}. \tag{23}$$

Proof. See Appendix B. □

Note that $\bar{\alpha}$ can be easily computed since it is independent of the CSI of the dual-hop channels. With the obtained $\bar{\alpha}$ and $\bar{P}_{\mathrm{out}}^{\mathrm{I}}$, the average throughput can be expressed as

$$\bar{R}_{\mathrm{HT}} = \frac{\eta g_r(\sqrt{\gamma_{\mathrm{th}}(\gamma_{\mathrm{th}}+1)}+\gamma_{\mathrm{th}})(1-\bar{P}_{\mathrm{out}}^{\mathrm{I}})\bar{F}_{g_1}\left(\frac{S_{\min}}{p_s}\right)R}{1+\eta g_r(\sqrt{\gamma_{\mathrm{th}}(\gamma_{\mathrm{th}}+1)}+\gamma_{\mathrm{th}})}. \tag{24}$$

As $p_s \to \infty$, we have $\bar{P}_{\mathrm{out}}^{\mathrm{I}} \to 0$, $\bar{F}_{g_1}\left(\frac{S_{\min}}{p_s}\right) \to 1$, and the asymptotic average throughput

$$\bar{R}_{\mathrm{HT}}^{\infty} \to \frac{\eta g_r(\sqrt{\gamma_{\mathrm{th}}(\gamma_{\mathrm{th}}+1)}+\gamma_{\mathrm{th}})R}{1+\eta g_r(\sqrt{\gamma_{\mathrm{th}}(\gamma_{\mathrm{th}}+1)}+\gamma_{\mathrm{th}})}. \tag{25}$$

In such a case, the asymptotic average throughput is independent of the CSI of the dual-hop channels and is a monotonically increasing function of g_r. Thus, a larger asymptotic average throughput is obtained with a larger g_r, which can alleviate the IC burden in the high p_s region if $\bar{\alpha}$ is applied.

When the QoS constraint Q_2 is considered, we denote by $F_y^{-1}(\varepsilon)$ the solution $2\sqrt{\xi}$ to the equation $F_y\left(2\sqrt{\xi}\right) = \varepsilon$ [27], so that $\xi = (F_y^{-1}(\varepsilon))^2/4$. Note that we have applied the fact $P_{\mathrm{out}}^{\mathrm{I}} = F_y\left(2\sqrt{\xi}\right)$ from (A.6) to obtain ξ; now we begin to characterize the optimal TS of (19) subject to Q_2.

Proposition 3. *For a given target information outage probability ε, the optimal TS factor that maximizes the average throughput subject to Q_2 in the HT model is given by*

$$\hat{\alpha} = \begin{cases} \frac{\hat{\kappa}}{\eta+\hat{\kappa}}, & g_r \le \hat{g}_r \\ \text{does not exsit}, & \text{otherwise}, \end{cases} \tag{26}$$

where $\hat{g}_r \triangleq \frac{p_s\theta_1\theta_2(F_y^{-1}(\varepsilon))^2}{4\gamma_{\mathrm{th}}\sigma_d^2\left(2\left(\gamma_{\mathrm{th}}+\sqrt{\gamma_{\mathrm{th}}(\gamma_{\mathrm{th}}+1)}\right)+1\right)}$ and $\hat{\kappa}$ is given by (27).

Proof. See Appendix C. □

Proposition 3 shows that $\hat{\alpha}$ does not exist and the target information outage probability cannot be achieved when $g_r > \hat{g}_r$. In such a case, the corresponding FDR transmission cannot be realized along with an e2e outage probability of 1. As can be seen from Appendix C, the information outage probability achieved by $\hat{\alpha}$ is $P_{\mathrm{out}}^{\mathrm{I}} = \varepsilon$ when $g_r \le \hat{g}_r$. With the obtained $\hat{\alpha}$ and $P_{\mathrm{out}}^{\mathrm{I}} = \varepsilon$, the average throughput given that $g_r \le \hat{g}_r$ can be expressed as

$$\hat{R}_{\mathrm{HT}} = \frac{(1-\varepsilon)\eta R\bar{F}_{g_1}\left(\frac{S_{\min}}{p_s}\right)}{\eta+\hat{\kappa}}. \tag{28}$$

As $p_s \to \infty$, we have $\hat{\kappa} \to 0$, $\bar{F}_{g_1}\left(\frac{S_{\min}}{p_s}\right) \to 1$, $\hat{g}_r \to \infty$, and $g_r < \hat{g}_r$. Thus, the asymptotic average throughput can be expressed as

$$\hat{R}_{\mathrm{HT}}^{\infty} \to (1-\varepsilon)R. \tag{29}$$

The expression in (29) implicitly shows that $\hat{\alpha} \to 0$ as $p_s \to \infty$. In other words, $\hat{\alpha}$ achieves an effective FDR transmission time of a whole block as $p_s \to \infty$, so that the asymptotic average throughput of (29) is the same as that of a corresponding conventional FDR network.

Corollary 1. *As $p_s \to \infty$, when $g_r < \frac{1-\varepsilon}{\eta\varepsilon\left(\sqrt{\gamma_{\mathrm{th}}(\gamma_{\mathrm{th}}+1)}+\gamma_{\mathrm{th}}\right)}$, $\bar{R}_{\mathrm{HT}}^{\infty} < \hat{R}_{\mathrm{HT}}^{\infty}$; otherwise, $\bar{R}_{\mathrm{HT}}^{\infty} \ge \hat{R}_{\mathrm{HT}}^{\infty}$.*

Proof. Comparing (25) and (29), it can be shown that $\bar{R}_{\mathrm{HT}}^{\infty} < \hat{R}_{\mathrm{HT}}^{\infty}$ has an equivalence $g_r < \frac{1-\varepsilon}{\eta\varepsilon\left(\sqrt{\gamma_{\mathrm{th}}(\gamma_{\mathrm{th}}+1)}+\gamma_{\mathrm{th}}\right)}$. Furthermore, it can be shown that $\bar{R}_{\mathrm{HT}}^{\infty} \ge \hat{R}_{\mathrm{HT}}^{\infty}$ has an equivalence $g_r \ge \frac{1-\varepsilon}{\eta\varepsilon\left(\sqrt{\gamma_{\mathrm{th}}(\gamma_{\mathrm{th}}+1)}+\gamma_{\mathrm{th}}\right)}$. This proves Corollary 1. □

Being consistent with contemporary wireless systems where an outage level near 1% is typical [27], [39], it can be shown that $\frac{1-\varepsilon}{\eta\varepsilon\left(\sqrt{\gamma_{\mathrm{th}}(\gamma_{\mathrm{th}}+1)}+\gamma_{\mathrm{th}}\right)} \gg 1$ with the substitution of practical η and γ_{th}, whereas g_r is less than 1 due to active/passive IC. Thus, we have $g_r < \frac{1-\varepsilon}{\eta\varepsilon\left(\sqrt{\gamma_{\mathrm{th}}(\gamma_{\mathrm{th}}+1)}+\gamma_{\mathrm{th}}\right)}$ in practice and the asymptotic average throughput achieved by $\hat{\alpha}$ is larger than that of $\bar{\alpha}$.

III. Harvest-Transmit-Store Model

In the HT model, all the harvested energy has been fully utilized for FDR transmission within each block, without considering energy accumulation and scheduling across channel realizations. Although the HT model is easy to implement, it would perform better if energy accumulation and scheduling were allowed to store a part of the harvested energy for future usage. Therefore, we propose a general HTS model with its GS implementation for the considered FDR-assisted SWIPT network. Note that a block-based HTS model has been proposed for HDR-assisted SWIPT networks in [32]. In contrast, our general HTS model achieves superior outage performance over that of the block-based HTS model. Furthermore, under

$$\hat{\kappa}=\frac{p_s\theta_1\theta_2(F_y^{-1}(\varepsilon))^2-4g_r\gamma_{\rm th}\sigma_d^2-\sqrt{\left(p_s\theta_1\theta_2(F_y^{-1}(\varepsilon))^2-4g_r\gamma_{\rm th}\sigma_d^2\right)^2-16p_s\theta_1\theta_2 g_r\gamma_{\rm th}^2\sigma_d^2(F_y^{-1}(\varepsilon))^2}}{2p_s\theta_1\theta_2 g_r\gamma_{\rm th}(F_y^{-1}(\varepsilon))^2}. \tag{27}$$

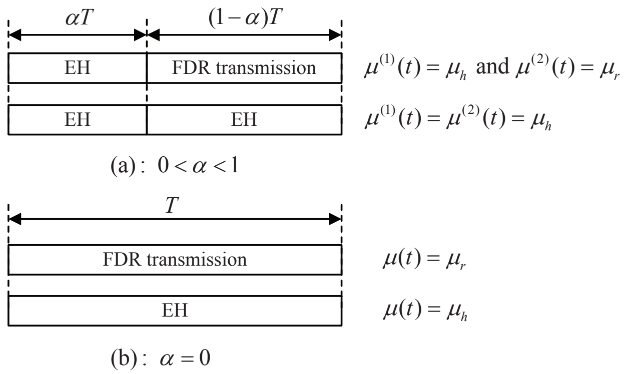

Fig. 2. Frame structure of the general HTS model: (a) $0<\alpha<1$ and (b) $\alpha=0$.

our analysis framework, the block-based HTS model can be treated as the special case $\alpha=0$.

The frame structure of the general HTS model is depicted in Fig. 2(a). In the first phase with a time duration αT, the relay switches to the EH mode μ_h. In the second phase with a time duration of $(1-\alpha)T$, the relay switches to the EH mode μ_h or the FDR transmission mode μ_r depending on the battery's residual energy level and CSI. Note that when $\alpha=0$, the frame structure of the general HTS model degenerates to that of the block-based HTS model, as depicted in Fig. 2(b). For intermediate and high SINRs, the e2e SINR of (9) can be approximated as [40]:

$$\gamma_{\rm e2e}\approx\min\{\gamma_{\rm R},\gamma_{\rm D}\}, \tag{30}$$

where $\gamma_{\rm R}=\frac{p_s g_1}{p_r g_r}$ is the SINR at the relay in the considered RSI dominated scenario. In order to decode the relaying signal received at the destination, it is required that the e2e SINR at least equals the target value $\gamma_{\rm th}$. Based on the above approximation, the required relay transmission power that ensures signal detection can be simplified to

$$p_r=\begin{cases}\frac{\gamma_{\rm th}\sigma_d^2}{g_2}, & \tilde{\gamma}_{\rm R}\geq\gamma_{\rm th}\\ \text{does not exist}, & \text{otherwise},\end{cases} \tag{31}$$

where $\tilde{\gamma}_{\rm R}\triangleq\frac{p_s g_1 g_2}{g_r\gamma_{\rm th}\sigma_d^2}$ denotes the SINR at the relay given that $p_r=\frac{\gamma_{\rm th}\sigma_d^2}{g_2}$ holds. Notably, the consumed energy for the relay transmission is $(1-\alpha)p_rT$. In the following, we again assume the time normalization of each block, so that we can consider energy and power interchangeably. Furthermore, we assume that a rechargeable battery has been employed at the relay with the battery size $p_b=\rho p_s$ $(\rho>0)$. The battery is discretized into $L+2$ energy levels $\varphi_i\triangleq ip_b/(L+1)$, where $i=0,1,\ldots,L+1$ [32], [41]. We define s_i, $i=0,1,\ldots,L+1$ as $L+2$ energy states of the battery, so that the battery is in the state s_i when its stored energy equals to φ_i.

Based on the considered discretized battery model, the energy that can be harvested during the first phase is defined as $\varphi_{h_1}\triangleq\varphi_{i^*_{h_1}}$, where

$$i^*_{h_1}=\arg\max_{i\in\{0,\ldots,L+1\}}\{\varphi_i:\varphi_i<\tilde{\varphi}_{h_1}\} \tag{32}$$

and $\tilde{\varphi}_{h_1}\triangleq\alpha\eta_h p_s g_1$. If the relay is operated in the EH mode μ_h in the second phase, the energy that can be harvested is defined as $\varphi_{h_2}\triangleq\varphi_{i^*_{h_2}}$, where

$$i^*_{h_2}=\arg\max_{i\in\{0,\ldots,L+1\}}\{\varphi_i:\varphi_i<\tilde{\varphi}_{h_2}\} \tag{33}$$

and $\tilde{\varphi}_{h_2}\triangleq(1-\alpha)\eta_h p_s g_1$. When the relay is operated in the FDR transmission mode μ_r in the second phase, the relay uses the stored energy to power its transmission. Corresponding to p_r of (31), the required energy level for transmission is given by

$$\varphi_r\triangleq\begin{cases}\varphi_{i^*_r}, & \text{if } \frac{(1-\alpha)p_r}{\eta_t}\leq p_b\\ \infty, & \text{otherwise},\end{cases} \tag{34}$$

where $i^*_r=\arg\min_{i\in\{1,\ldots,L+1\}}\left\{\varphi_i:\varphi_i\geq\frac{(1-\alpha)p_r}{\eta_t}\right\}$. In each block, an outage event occurs when the source signal cannot be decoded at the destination or equivalently when the relay is operating in the EH mode μ_h in the second phase. Thus, the main optimization target is to minimize the number of times that the relay does not perform FDR transmission in the second phase. To this end, the GS policy prioritizes the operation modes μ_r in the second phase of each block. At the beginning of the second phase, when the residual energy of the battery can support the required transmitted energy, the GS policy switches the relay node to FDR transmission; otherwise it switches the relay node to EH. On denoting the battery's residual energy levels at the beginnings of the first and second phases of the tth block by $E_1(t)\in\{\varphi_i:0\leq i\leq L+1\}$ and $E_2(t)\in\{\varphi_i:0\leq i\leq L+1\}$, respectively, the GS policy can be expressed as $\mu^{(1)}(t)=\mu_h$ for the first phase and

$$\mu^{(2)}(t)=\begin{cases}\mu_r, & (E_2(k)\geq\varphi_r)\cap(\tilde{\gamma}_{\rm R}\geq\gamma_{\rm th})\\ \mu_h, & ((E_2(k)<\varphi_r)\cap(\tilde{\gamma}_{\rm R}\geq\gamma_{\rm th}))\cup(\tilde{\gamma}_{\rm R}<\gamma_{\rm th})\end{cases} \tag{35}$$

for the second phase, respectively. Furthermore, the battery's residual energy levels can be expressed as

$$E_2(t)=\min\{p_b,E_1(t)+\varphi_{h_1}\} \tag{36}$$

and

$$E_1(t+1)=\min\{p_b,E_2(t)+w\varphi_{h_2}+(1-w)\varphi_r\}, \tag{37}$$

where

$$w=\begin{cases}1, & \mu^{(2)}(t)=\mu_h\\ 0, & \mu^{(2)}(t)=\mu_r.\end{cases} \tag{38}$$

A. MC for the GS Policy

For the GS policy, a specific harvesting/relaying behavior of the relay's battery can be modeled as a specific state-transition of a finite-state MC, so that the energy level of the relay's battery at the beginning of each block represents a specific state of the MC. Since the GS policy switches the relay to the mode μ_h in the first phase and to the mode μ_h or μ_r in the second phase, the MC model has a two-stage transition for each block.

Assume that the initial, intermediate, and final states of the battery's energy level in each block are s_i, s_k, and s_j, respectively, the transitions $s_i \to s_k$ and $s_k \to s_j$ occur in the first and second phases, respectively, and the transition $s_i \to s_k \to s_j$ occurs throughout the whole block. In the first phase, we have $k \geq i$ due to the EH operation. In the second phase, we have $k > j$ if the relay is operated in the mode μ_r or $k \leq j$ if the relay is operated in the mode μ_h. It can be shown that an outage event occurs when $k \leq j$ for $s_i \to s_k \to s_j$ and a non-outage event occurs when $k > j$ for $s_i \to s_k \to s_j$. The transition matrix of the MC can be denoted by $\boldsymbol{P} \in \mathbb{R}^{(L+2)\times(L+2)}$ with its ith-row and jth-column element $P_{i,j}$ representing the probability of the transition from the state s_i to the state s_j in a transmission block. Similarly, we define $P^{(1)}_{i,k}$ as the transition probability in the first phase and define $\bar{P}^{(2)}_{k,j}$ and $\tilde{P}^{(2)}_{k,j}$ as the transition probabilities in the second phase for $k \leq j$ and $k > j$, respectively. With respect to the two-stage state transition, $P_{i,j}$ can be written as

$$\begin{aligned} P_{i,j} &\triangleq \sum_{k\leq j} P^{(1)}_{i,k}\bar{P}^{(2)}_{k,j} + \sum_{k>j} P^{(1)}_{i,k}\tilde{P}^{(2)}_{k,j} \\ &\triangleq \bar{P}_{i,j} + \tilde{P}_{i,j}, \end{aligned} \tag{39}$$

where $\bar{P}_{i,j} \triangleq \sum_{k\leq j} P^{(1)}_{i,k}\bar{P}^{(2)}_{k,j}$ and $\tilde{P}_{i,j} \triangleq \sum_{k>j} P^{(1)}_{i,k}\tilde{P}^{(2)}_{k,j}$ are the transition probabilities corresponding to an outage event and a non-outage event, respectively. Based on (39), the transition probabilities of the MC are determined in the following:

1) The Empty Battery Remains Empty ($s_0 \to s_k \to s_0$): In this case, an outage event occurs for $s_0 \to s_0 \to s_0$ and a non-outage event occurs for $s_0 \to s_k \to s_0$ with $1 \leq k \leq L+1$. Thus, the transition probabilities corresponding to an outage event and a non-outage event are respectively given by $\bar{P}_{0,0} = P^{(1)}_{0,0}\bar{P}^{(2)}_{0,0}$ and $\tilde{P}_{0,0} = \sum_{k=1}^{L+1} P^{(1)}_{0,k}\tilde{P}^{(2)}_{k,0}$, where

$$\begin{aligned} P^{(1)}_{0,k} &= \begin{cases} \Pr\{\tilde{\varphi}_{h_1} < \varphi_1\}, & k=0 \\ \Pr\{\tilde{\varphi}_{h_1} \geq p_b\}, & k=L+1 \\ \Pr\{\varphi_k \leq \tilde{\varphi}_{h_1} < \varphi_{k+1}\}, & \text{otherwise} \end{cases} \\ &= \begin{cases} F_{g_1}\left(\frac{\varphi_1}{\alpha\eta_h p_s}\right), & k=0 \\ \bar{F}_{g_1}\left(\frac{p_b}{\alpha\eta_h p_s}\right), & k=L+1 \\ F_{g_1}\left(\frac{\varphi_{k+1}}{\alpha\eta_h p_s}\right) - F_{g_1}\left(\frac{\varphi_k}{\alpha\eta_h p_s}\right), & \text{otherwise,} \end{cases} \end{aligned} \tag{40}$$

$$\bar{P}^{(2)}_{0,0} = \Pr\{\tilde{\varphi}_{h_2} < \varphi_1\} = F_{g_1}\left(\frac{\varphi_1}{(1-\alpha)\eta_h p_s}\right), \tag{41}$$

and

$$\begin{aligned} \tilde{P}^{(2)}_{k,0} &= \Pr\{(\varphi_{k-1} < \varphi_r \leq \varphi_k) \cap (\tilde{\gamma}_{\rm R} \geq \gamma_{\rm th})\} \\ &= \bar{F}_y\left(\frac{g_r\gamma_{\rm th}^2\sigma_d^2}{p_s\theta_1\theta_2}\right)\left(F_{g_2}\left(\frac{(1-\alpha)\gamma_{\rm th}\sigma_d^2}{\eta_t\varphi_{k-1}}\right) - F_{g_2}\left(\frac{(1-\alpha)\gamma_{\rm th}\sigma_d^2}{\eta_t\varphi_k}\right)\right). \end{aligned} \tag{42}$$

Then, the transition probability for this case is given by $P_{0,0} = \bar{P}_{0,0} + \tilde{P}_{0,0}$.

2) The Empty Battery Is Partially Charged ($s_0 \to s_k \to s_j$: $0 < j < L+1$): In this case, an outage event occurs when $0 \leq k \leq j$ and a non-outage event occurs when $j+1 \leq k \leq L+1$. The corresponding transition probabilities are respectively given by $\bar{P}_{0,j} = \sum_{k=0}^{j} P^{(1)}_{0,k}\bar{P}^{(2)}_{k,j}$ and $\tilde{P}_{0,j} = \sum_{k=j+1}^{L+1} P^{(1)}_{0,k}\tilde{P}^{(2)}_{k,j}$, where $P^{(1)}_{0,k}$ is given by (40),

$$\begin{aligned} \bar{P}^{(2)}_{k,j} &= \Pr\{(\varphi_j - \varphi_k \leq \tilde{\varphi}_{h_2} < \varphi_{j+1} - \varphi_k) \cap \\ &\qquad (((\varphi_k < \varphi_r) \cap (\tilde{\gamma}_{\rm R} \geq \gamma_{\rm th})) \cup (\tilde{\gamma}_{\rm R} < \gamma_{\rm th}))\} \\ &= \left(F_{g_1}\left(\frac{\varphi_{j+1}-\varphi_k}{(1-\alpha)\eta_h p_s}\right) - F_{g_1}\left(\frac{\varphi_j-\varphi_k}{(1-\alpha)\eta_h p_s}\right)\right) \\ &\qquad \left(F_{g_2}\left(\frac{(1-\alpha)\gamma_{\rm th}\sigma_d^2}{\eta_t\varphi_k}\right)\bar{F}_y\left(\frac{g_r\gamma_{\rm th}^2\sigma_d^2}{p_s\theta_1\theta_2}\right) + F_y\left(\frac{g_r\gamma_{\rm th}^2\sigma_d^2}{p_s\theta_1\theta_2}\right)\right), \end{aligned} \tag{43}$$

and

$$\begin{aligned} \tilde{P}^{(2)}_{k,j} &= \Pr\{(\varphi_k - \varphi_{j+1} < \varphi_r \leq \varphi_k - \varphi_j) \cap (\tilde{\gamma}_{\rm R} \geq \gamma_{\rm th})\} \\ &= \bar{F}_y\left(\frac{g_r\gamma_{\rm th}^2\sigma_d^2}{p_s\theta_1\theta_2}\right)\left(F_{g_2}\left(\frac{(1-\alpha)\gamma_{\rm th}\sigma_d^2}{\eta_t(\varphi_k-\varphi_{j+1})}\right) - F_{g_2}\left(\frac{(1-\alpha)\gamma_{\rm th}\sigma_d^2}{\eta_t(\varphi_k-\varphi_j)}\right)\right). \end{aligned} \tag{44}$$

Then, the transition probability for this case is given by $P_{0,j} = \bar{P}_{0,j} + \tilde{P}_{0,j}$.

3) The Empty Battery Is Fully Charged ($s_0 \to s_k \to s_{L+1}$): This is the scenario in which the empty battery becomes fully charged at the end of a transmission block. In such a case, the transition probability corresponding to an outage event is given by

$$\bar{P}_{0,L+1} = \sum_{k=0}^{L+1} P^{(1)}_{0,k}\bar{P}^{(2)}_{k,L+1}, \tag{45}$$

where $P^{(1)}_{0,k}$ is given by (40) and $\bar{P}^{(2)}_{k,L+1}$ is given by

$$\begin{aligned} \bar{P}^{(2)}_{k,L+1} &= \Pr\{(((\varphi_k < \varphi_r) \cap (\tilde{\gamma}_{\rm R} \geq \gamma_{\rm th})) \cup (\tilde{\gamma}_{\rm R} < \gamma_{\rm th})) \cap \\ &\qquad (\tilde{\varphi}_{h_2} \geq p_b - \varphi_k)\} \\ &= \left(F_{g_2}\left(\frac{(1-\alpha)\gamma_{\rm th}\sigma_d^2}{\eta_t\varphi_k}\right)\bar{F}_y\left(\frac{g_r\gamma_{\rm th}^2\sigma_d^2}{p_s\theta_1\theta_2}\right) + F_y\left(\frac{g_r\gamma_{\rm th}^2\sigma_d^2}{p_s\theta_1\theta_2}\right)\right) \\ &\qquad \bar{F}_{g_1}\left(\frac{p_b-\varphi_k}{(1-\alpha)\eta_h p_s}\right). \end{aligned} \tag{46}$$

Furthermore, the transition probability corresponding to a non-outage event is given by $\tilde{P}_{0,L+1} = 0$ due to the absence of discharging in the second phase. Then, the transition probability of this case can be expressed as $P_{0,L+1} = \bar{P}_{0,L+1}$.

4) The Battery Remains Full ($s_{L+1} \to s_{L+1} \to s_{L+1}$): This case corresponds to the scenarios in which the battery is fully charged at the beginning of the first phase, so that the battery cannot harvest more energy. In the second phase, a) the required transmitted energy is higher than the battery size given that $\tilde{\gamma}_{\rm R} \geq \gamma_{\rm th}$ or b) $\tilde{\gamma}_{\rm R} < \gamma_{\rm th}$. In such a case, $\bar{P}_{L+1,L+1} = P^{(1)}_{L+1,L+1}\bar{P}^{(2)}_{L+1,L+1}$, where $P^{(1)}_{L+1,L+1} = 1$ and $\bar{P}^{(2)}_{L+1,L+1}$ can be obtained by substituting $k = L+1$ and $\varphi_{L+1} = p_b$ into (46). Thus, we have

$$\bar{P}_{L+1,L+1} = F_{g_2}\left(\frac{(1-\alpha)\gamma_{\rm th}\sigma_d^2}{\eta_t p_b}\right)\bar{F}_y\left(\frac{g_r\gamma_{\rm th}^2\sigma_d^2}{p_s\theta_1\theta_2}\right) + F_y\left(\frac{g_r\gamma_{\rm th}^2\sigma_d^2}{p_s\theta_1\theta_2}\right). \tag{47}$$

Furthermore, we have $\tilde{P}_{L+1,L+1} = 0$ due to the absence of discharging in the second phase. Therefore, the transition probability for this case can be expressed as $P_{L+1,L+1} = \bar{P}^{(2)}_{L+1,L+1}$.

5) The Non-Empty and Non-Full Battery Remains Unchanged ($s_i \to s_k \to s_i$: $0 < i < L+1$): In this case, the transition probability corresponding to an outage event is $\bar{P}_{i,i} = P^{(1)}_{i,i}\bar{P}^{(2)}_{i,i}$, where

$$P^{(1)}_{i,i} = \Pr\{\tilde{\varphi}_{h_1} < \varphi_1\} = F_{g_1}\left(\frac{\varphi_1}{\alpha\eta_h p_s}\right) \tag{48}$$

and $\bar{P}^{(2)}_{i,i}$ is obtained from (43) with the substitution $k = j = i$ in it, i.e.,

$$\begin{aligned}\bar{P}^{(2)}_{i,i} = &F_{g_1}\left(\frac{\varphi_1}{(1-\alpha)\eta_h p_s}\right)\\ &\left(F_{g_2}\left(\frac{(1-\alpha)\gamma_{\rm th}\sigma_d^2}{\eta_t\varphi_i}\right)\bar{F}_y\left(\frac{g_r\gamma_{\rm th}^2\sigma_d^2}{p_s\theta_1\theta_2}\right)+F_y\left(\frac{g_r\gamma_{\rm th}^2\sigma_d^2}{p_s\theta_1\theta_2}\right)\right).\end{aligned} \tag{49}$$

The transition probability corresponding to a non-outage event is $\tilde{P}_{i,i} = \sum_{k=i+1}^{L+1} P^{(1)}_{i,k}\tilde{P}^{(2)}_{k,i}$, where

$$\begin{aligned}P^{(1)}_{i,k} &= \begin{cases}\Pr\{\tilde{\varphi}_{h_1} \geq p_b - \varphi_i\}, & k = L+1\\ \Pr\{\varphi_k - \varphi_i \leq \tilde{\varphi}_{h_1} < \varphi_{k+1} - \varphi_i\}, & \text{otherwise}\end{cases}\\ &= \begin{cases}\bar{F}_{g_1}\left(\frac{p_b-\varphi_i}{\alpha\eta_h p_s}\right), & k = L+1\\ F_{g_1}\left(\frac{\varphi_{k+1}-\varphi_i}{\alpha\eta_h p_s}\right) - F_{g_1}\left(\frac{\varphi_k-\varphi_i}{\alpha\eta_h p_s}\right), & \text{otherwise}\end{cases}\end{aligned} \tag{50}$$

and $\tilde{P}^{(2)}_{k,i}$ is obtained from (44) with the substitution $j = i$ in it. Then, the transition probability for this case can be expressed as $P_{i,i} = \bar{P}_{i,i} + \tilde{P}_{i,i}$.

6) The Non-Empty and Non-Full Battery Is Fully Charged ($s_i \to s_k \to s_{L+1}$: $0 < i < L+1$): In this case, we have $\tilde{P}_{i,L+1} = 0$ due to the absence of discharging. Then, the transition probability is given by

$$P_{i,L+1} = \bar{P}_{i,L+1} = \sum_{k=i}^{L+1} P^{(1)}_{i,k}\bar{P}^{(2)}_{k,L+1}, \tag{51}$$

where $P^{(1)}_{i,k}$ is given by (50) and $\bar{P}^{(2)}_{k,L+1}$ is the same as that of the case 3).

7) The Non-Empty and Non-Full Battery Is Partially Charged ($s_i \to s_k \to s_j$: $0 < i < j < L+1$): In this case, the transition probabilities corresponding to an outage event and a non-outage event are respectively given by

$$\bar{P}_{i,j} = \sum_{k=i}^{j} P^{(1)}_{i,k}\bar{P}^{(2)}_{k,j} \ \text{ and } \ \tilde{P}_{i,j} = \sum_{k=j+1}^{L+1} P^{(1)}_{i,k}\tilde{P}^{(2)}_{k,j}, \tag{52}$$

where $P^{(1)}_{i,k}$ is given by (50), $\bar{P}^{(2)}_{k,j}$ is given by (43), and $\tilde{P}^{(2)}_{k,j}$ is given by (44). Then, the transition probability of this case can be expressed as $P_{i,j} = \bar{P}_{i,j} + \tilde{P}_{i,j}$.

8) The Non-Empty Battery Is Discharged ($s_i \to s_k \to s_j$: $0 \leq j < i \leq L+1$): In this case, we have $\bar{P}_{i,j} = 0$ since the battery always discharges with respect to $j < i$. Thus, the transition probability can be expressed as

$$P_{i,j} = \tilde{P}_{i,j} = \sum_{k=i}^{L+1} P^{(1)}_{i,k}\tilde{P}^{(2)}_{k,j}, \tag{53}$$

where $P^{(1)}_{i,k}$ is given by (50) and $\tilde{P}^{(2)}_{k,j}$ is given by (44).

B. Stationary Distribution and System Performance

In order to explore how the relay's battery is charged and discharged according to the GS policy, the stationary distribution of the MC needs to be derived in order to determine the e2e outage probability.

Proposition 4. *The state transition matrix $\boldsymbol{P} = (P_{i,j})$ of the MC that models the battery's behavior is irreducible and row stochastic.*

Proof. The proof is similar to that of Proposition 1 of [32]. □

Since that the transition matrix $\boldsymbol{P}$ is irreducible and row stochastic, the stationary distribution of the MC can be computed by [42]

$$\boldsymbol{\pi} = (\boldsymbol{P}^T - \boldsymbol{I} + \boldsymbol{B})^{-1}\boldsymbol{b}, \tag{54}$$

where the element of the $(L+2)\times(L+2)$ matrix $\boldsymbol{B}$ in its i-th row and j-th column is given by $B_{i,j} = 1\ \forall i,j$ and $\boldsymbol{b} = [1,1,\ldots,1]^T$ is an $(L+2)\times 1$ vector. With respect to the two-stage transition in each block, an outage event occurs when the battery does not discharge in the second phase of a block, which transits the battery's state to a non-decreased energy level in the second phase, i.e., $k \leq j$ for $s_i \to s_k \to s_j$, and the corresponding transition probability is $\bar{P}_{i,j}$. Therefore, the e2e outage probability achieved by the GS policy can be expressed as

$$P^{(\rm GS)}_{\rm out} = \sum_{i=0}^{L+1}\pi_i\sum_{j=i}^{L+1}\bar{P}_{i,j}. \tag{55}$$

The average throughput and the successful rate achieved by the GS policy can be respectively expressed as

$$R_{\rm GS} = (1-\alpha)(1-P^{\rm GS}_{\rm out})R \tag{56}$$

and

$$R^{(s)}_{\rm GS} = \begin{cases}(1-\alpha)(1-\varepsilon)R, & P^{(\rm GS)}_{\rm out} \leq \varepsilon\\ 0, & \text{otherwise.}\end{cases} \tag{57}$$

By comparing our proposed general HTS model with the block-based HTS model proposed in [32], it can be shown that the general HTS model degenerates to the block-based HTS model when $\alpha = 0$. Thus, our analysis framework can be directly applied to the block-based HTS model for the considered FDR-assisted SWIPT network and the corresponding e2e outage probability can be computed by substituting $\alpha = 0$ into the above analysis framework. Due to the complicated computation of the stationary distribution, the optimal TS that maximizes the average throughput subject to the QoS constraints can hardly be obtained in closed form for the general HTS model. Thus, in maximizing the QoS-constrained average throughput (successful rate) for the general HTS model, we choose α intuitively based on numerical results as discussed in the following section.

IV. Numerical Results

This section presents some numerical results to validate the performance results of the developed schemes. In the simulations, the EH receiver sensitivity is set as $\varphi_{\min} = -27$

TABLE I
SIMULATION PARAMETERS

No.	Parameter	Value
1	Carrier frequency	868 MHz
2	Fixed transmission rate R	3 bps/Hz
3	Target information outage probability ε	1%
4	$\mathcal{L}$ at $d_0 = 1$ m	-30 dB
5	Distances of dual-hop links: d_1 and d_2	8 and 18 m
6	Path loss exponent φ	2.5
7	Souce/relay transmit antenna gain	18/8 dB
8	Additive noise power: $\sigma_r^2 = \sigma_d^2$	-90 dBm
9	Energy coefficients: η_h and η_t	0.4 and 0.75

dBm [37] and the size of the relay's battery is set as $p_b = \rho p_s$, where $\rho = m_1\theta_1$. Considering $\varphi_1 \geq \varphi_{\min}$ in practice, we set the actual number of energy levels of the relay's battery to $\tilde{L}+2$, where $\tilde{L} \triangleq \min\{L, \lfloor p_b/\varphi_{\min}\rfloor - 1\}$. For the sake of simplicity, we use the terms general HTS model and the GS policy interchangeably in the following. Furthermore, the optimal solution of (13) without any QoS constraint is denoted by α^*. Unless otherwise stated, the remaining parameters used in the simulations are given in Table 1.

Fig. 3 investigates the e2e outage probability versus α of the considered schemes. In Fig. 3, we set $p_s = 26$ dBm, $g_r = -10$ dB, $m_1 = 4$, and $m_2 = 2$. As observed in Fig. 3, the e2e outage probability of the HT model first decreases with increasing α. After reaching a minimum, the e2e outage probability of the HT model begins to increase with increasing α. Furthermore, the e2e outage probability exhibits a piecewise behavior and approaches 1 in the high α region, as indicated by Proposition 1. Note that the HT model suffers serious outage performance degradation in the low and high α regions. As expected, when $\bar{\alpha}$ is applied, the achieved e2e outage probability is $P_{\rm out} = 0.005$, which matches the minimum value of that of the HT model. When $\hat{\alpha}$ is applied, Fig. 3 shows that the target outage probability $\varepsilon = 0.01$ has been maintained. For the general HTS model, Fig. 3 shows that $\alpha = 0$ achieves the worst outage performance over all values of α. Note that $\alpha = 0$ corresponds to the block-based HTS model. As α increases from 0 to the high α region, it can be shown the e2e outage probability first decreases dramatically and then approaches an outage floor of 0.003. Notably, the general HTS model achieves the best outage performance over α (note that $\bar{\alpha}$ and $\hat{\alpha}$ are fixed).

The average throughput versus α of the considered schemes is depicted in Fig. 4, where the simulation parameters are the same as those of Fig. 3. Fig. 4 clearly shows that the maximum average throughput of the HT model is achieved by $\alpha^* = 0.17$. Recalling the e2e outage performance in Fig. 3, it can be shown that the maximum average throughput of the HT model is achieved with $P_{\rm out} \approx 0.1$, so that the outage performance seriously degrades compared to $\varepsilon = 0.01$. Although $\bar{\alpha}$ and $\hat{\alpha}$ achieve a lower average throughput than the maximum point in the HT model, the corresponding outage performance is acceptable, as depicted in Fig. 3. Furthermore, $\hat{\alpha}$ achieves a higher average throughput than that of $\bar{\alpha}$. For the general HTS model, Fig. 4 shows that the maximum average throughput is achieved by $\alpha = 0$. Unfortunately, we know that the corresponding outage performance is not acceptable by recalling the results of Fig. 3, so that the maximum average throughput achieved by $\alpha = 0$ is not useful. As α increases from 0, the achieved average throughput first decreases slowly and then maintains a fixed rate of decrease. Notably, the GS implementation of the general HTS model always achieves a higher average throughput than that of the HT model for all α.

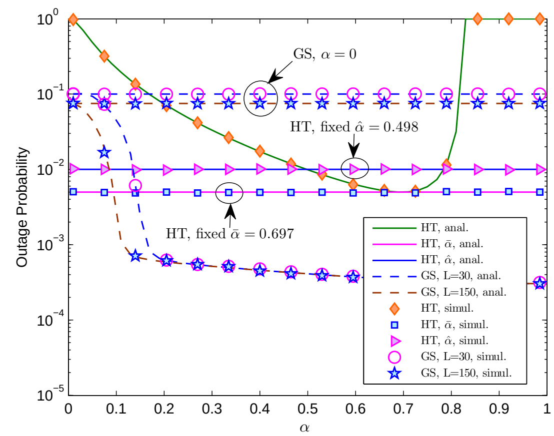

Fig. 3. Outage probability versus α.

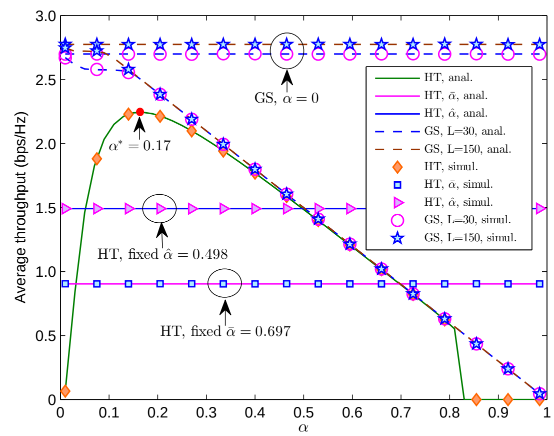

Fig. 4. Average throughput versus α.

Fig. 5 shows the successful rate versus α of the considered schemes corresponding to Fig. 3 and Fig. 4. It is seen from Fig. 5 that the so-called optimal $\alpha^* = 0.17$ for the HT model achieves a zero successful rate due to the associated poor outage performance. Both $\bar{\alpha}$ and $\hat{\alpha}$ achieve a non-zero successful rate. The GS policy achieves the highest successful rate for α. Furthermore, the non-zero successful rate achieved by the GS policy corresponds to a wider α region than that of the HT model. When $\alpha = 0$, the GS policy achieves a zero successful rate. Therefore, it can be summarized that the general HTS model can maximize the successful rate among all the considered schemes by setting a non-zero TS factor.

The impact of g_r on the e2e outage probability is depicted in Fig. 6, where we set $m_1 = 4$, $m_2 = 2$, and $p_s = 26$ dBm. As observed, the e2e outage probabilities of all the considered schemes increase with increasing g_r. For the HT model, the numerically optimized α^* achieves the worst outage performance in the low and middle g_r regions. Fig. 6 also shows

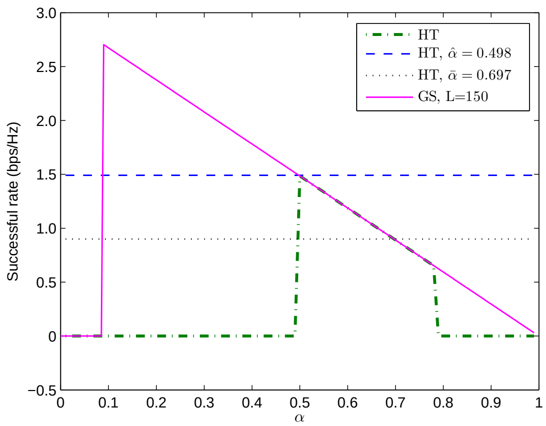

Fig. 5. Successful rate versus α.

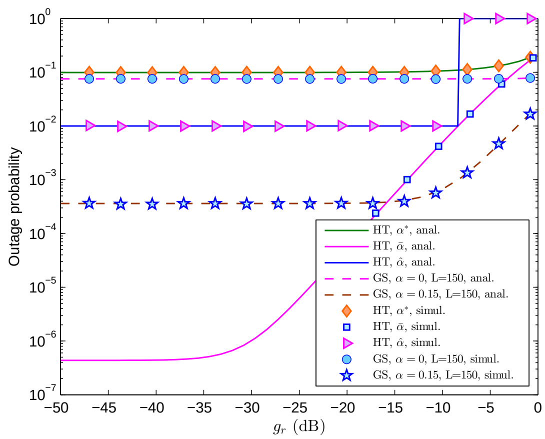

Fig. 6. Outage probability versus g_r.

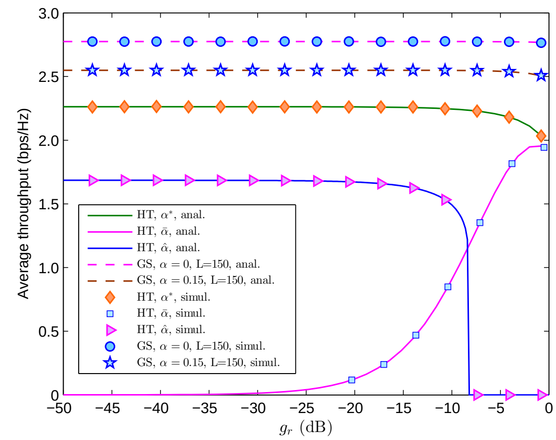

Fig. 7. Average throughput versus g_r.

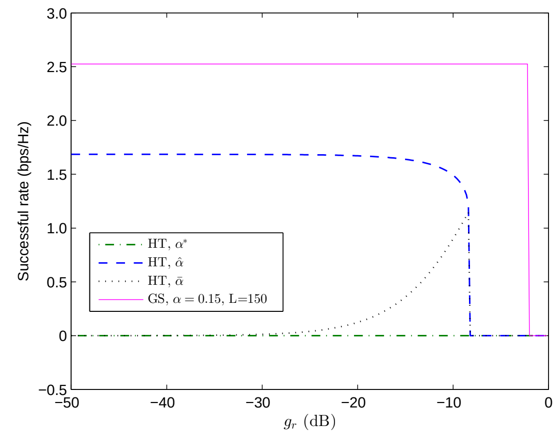

Fig. 8. Successful rate versus g_r.

that the e2e outage probability achieved by $\hat{\alpha}$ experiences a piecewise behavior, as suggested by Proposition 3. For the HT model, the best e2e outage performance is achieved by $\bar{\alpha}$. In the low g_r region, $\bar{\alpha}$ results in an outage floor due to the fact that $\bar{\alpha} \to 1$ as $g_r \to 0$. For the HTS model, the GS policy with $\alpha = 0$ achieves a poor outage performance. Furthermore, in the high p_r region, the GS policy with $\alpha = 0.15$ achieves the best outage performance among all the considered schemes.

The average throughput versus g_r is depicted in Fig. 7, in which the simulation parameters are the same as those of Fig. 6. As observed in Fig. 7, except for $\bar{\alpha}$, the average throughputs achieved by all the schemes decrease with increasing of g_r. For $\bar{\alpha}$, the obtained average throughput increases with increasing g_r, which is consistent with the asymptotic analysis of the average throughput of Proposition 2. For the HT model, although α^* achieves the highest average throughput, we know that it has poor outage performance by recalling the results of Fig. 6. Fortunately, the GS policy achieves a higher average throughput than that of the HT model for all g_r. Note that the average throughput achieved by the GS policy with $\alpha = 0$ is higher than that of the GS policy with $\alpha = 0.15$, whereas the corresponding outage performance is worse than that of the latter.

Fig. 8 shows the successful rate versus g_r of the considered schemes corresponding to Fig. 6 and Fig. 7. Fig. 8 shows that the so-called optimal α^* for the HT model achieves a zero successful rate. In the low and middle g_r regions, the successful rate achieved by $\hat{\alpha}$ is higher than that of $\bar{\alpha}$. In the high g_r region, both $\hat{\alpha}$ and $\bar{\alpha}$ achieve a zero successful rate. Notably, the GS policy with $\alpha = 0.15$ achieves the highest successful rate among all the considered schemes. Only when g_r becomes larger than -2 dB, does the GS policy with $\alpha = 0.15$ achieve a zero successful rate.

Fig. 9 shows the e2e outage probability versus p_s. In Fig. 9, we set $m_1 = 4$, $m_2 = 2$, and $g_r = -10$ dB. As observed, the piecewise behavior occurs for the e2e outage probability achieved by $\hat{\alpha}$. For the HT model, the best outage performance is achieved by $\bar{\alpha}$ for the considered values of p_s. For the HTS model, the GS policy with $\alpha = 0$ approaches an outage floor with increasing p_s. Moreover, the best outage performance is achieved by the GS policy with $\alpha = 0.15$ in the middle and high p_s regions among all the considered schemes.

The average throughput versus p_s is shown in Fig. 10, where the simulation parameters are the same as those of Fig. 9. As observed in Fig. 10, α^* achieves the highest average throughput among all the schemes in the HT model. However, the highest average throughput achieved by α^* also results in a poor outage performance as depicted in Fig. 9. As expected from Corollary 1, Fig. 10 shows that $\hat{\alpha}$ achieves a higher average throughput than that of $\bar{\alpha}$ in the high p_s region. For the general HTS model, Fig. 10 also shows that although the GS policy with $\alpha = 0$ achieves the highest average throughput,

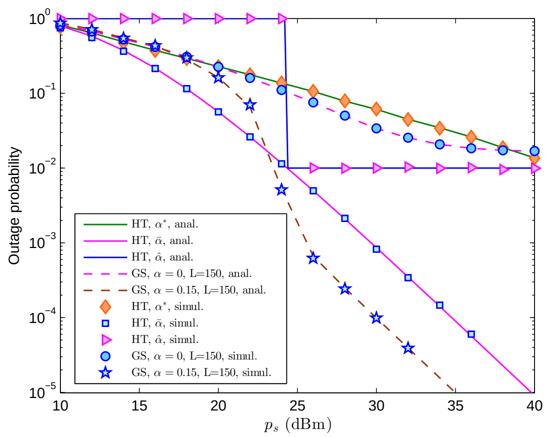

Fig. 9. Outage probability versus p_s.

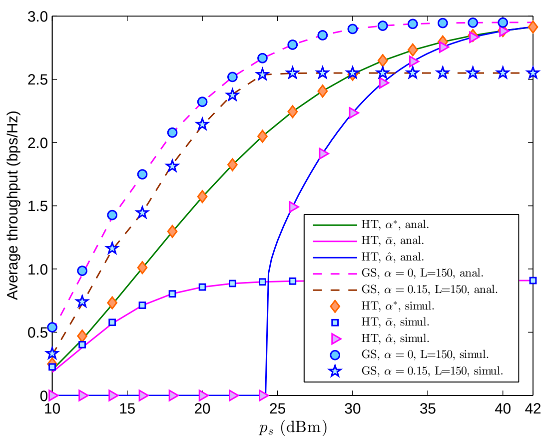

Fig. 10. Average throughput versus p_s.

the corresponding outage performance degenerates seriously, as depicted in Fig. 9. Notably, in the low and middle p_s regions, the GS policy with $\alpha = 0.15$ achieves a higher average throughput than all the schemes of the HT model.

Fig. 11 shows the successful rate versus p_s of the considered schemes corresponding to Fig. 9 and Fig. 10. Fig. 11 shows that the so-called optimal α^* for the HT model achieves a zero successful rate in most of the considered p_s region. For the HT model, $\hat{\alpha}$ always achieves a higher non-zero successful rate than that of $\bar{\alpha}$ for the considered range of p_s. Furthermore, the GS policy achieves a higher non-zero successful rate than that of $\hat{\alpha}$ in the middle p_s region. However, in the high p_s region, $\hat{\alpha}$ achieves a higher non-zero successful rate than that of the GS policy. The reason for this phenomenon is that we set the fixed $\alpha = 0.15$ for the GS policy intuitively, whereas $\hat{\alpha}$ becomes smaller with increasing p_s.

V. Conclusion

This paper has studied QoS-constrained relay control for an FDR-assisted SWIPT network in terms of the e2e outage probability, average throughput, and successful rate. Conditioned on the RSI channel power, the e2e outage probability has been derived for the HT model. Subject to the QoS-constraints of minimizing outage probability and maintaining a target outage probability, two optimal TS factors that maximize the average throughput have been respectively presented for the HT model. To enable energy accumulation and scheduling across channel realizations, the general HTS model has been proposed by employing TS within each transmission block. To analyze the e2e outage probability of the general HTS model, the residual energy levels of the relay's battery have been modeled as an MC with a two-stage state transition. Based on this uniform framework, the block-based HTS model can be analyzed as a special case of the general HTS model. The practical significance of the proposed QoS-constrained control schemes over the HT model without the QoS-constraints and the block-based HTS model has been verified by numerical results.

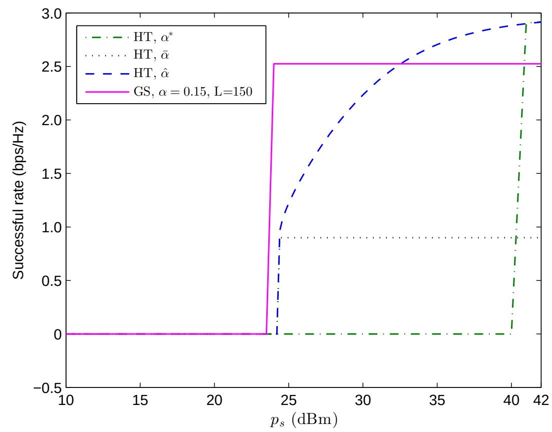

Fig. 11. Successful rate versus p_s.

Appendix A: A proof of Proposition 1

The e2e outage probability can be rewritten as

$$P_{\text{out}}^{(\text{HT})} = \Pr\left\{g_1 < \frac{S_{\min}}{p_s}\right\} + \Pr\left\{\left(g_1 \geq \frac{S_{\min}}{p_s}\right) \cap \left(\gamma_{\text{e2e}} < \gamma_{\text{th}}\right)\right\}. \quad (A.1)$$

Since g_1 follows the gamma distribution, we have

$$\Pr\left\{g_1 < \frac{S_{\min}}{p_s}\right\} = F_{g_1}\left(\frac{S_{\min}}{\theta_1}\right) = 1 - \frac{\Gamma_u\left(m_1, \frac{S_{\min}}{p_s\theta_1}\right)}{\Gamma(m_1)} \quad (A.2)$$

and

$$\Pr\left\{g_1 \geq \frac{S_{\min}}{p_s}\right\} = \bar{F}_{g_1}\left(\frac{S_{\min}}{\theta_1}\right) = \frac{\Gamma_u\left(m_1, \frac{S_{\min}}{p_s\theta_1}\right)}{\Gamma(m_1)}. \quad (A.3)$$

Then, the task is to evaluate $P_{\text{out}}^{\text{I}} = \Pr\{\gamma_{\text{e2e}} < \gamma_{\text{th}}\}$. By substituting (9) into $P_{\text{out}}^{\text{I}} = \Pr\{\gamma_{\text{e2e}} < \gamma_{\text{th}}\}$, conditioned on the RSI channel power, $P_{\text{out}}^{\text{I}}$ can be expressed as

$$P_{\text{out}}^{\text{I}} = \begin{cases} \Pr\left\{g_1 g_2 < \frac{\gamma_{\text{th}}\sigma_d^2(1+\kappa g_r)}{\kappa p_s(1-\kappa\gamma_{\text{th}} g_r)}\right\}, & g_r < \frac{1}{\kappa\gamma_{\text{th}}} \\ 1, & g_r \geq \frac{1}{\kappa\gamma_{\text{th}}} \end{cases}. \quad (A.4)$$

Define $x_i \triangleq g_i/\theta_i$ for $i = 1, 2$ and $y \triangleq x_1 x_2$. Notably, x_i ($i = 1$ and 2) has the standard gamma distribution and y is the product of two independent gamma variables. By utilizing the result of [43], the CDF of y can be shown as

$$F_y(y) = \frac{2^{2-m_1-m_2}}{\Gamma(m_1)\Gamma(m_2)} D_{\mu,\nu}(2\sqrt{y}), \quad (A.5)$$

where $\mu = m_1 + m_2 - 1$, $\nu = m_1 - m_2$, and $D_{\mu,\nu}(y) = \int_0^y x^{\mu} K_{\nu}(x)\mathrm{d}x$. Then, conditioned on g_r, $P_{\text{out}}^{\mathrm{I}}$ can be further expressed as

$$
\begin{aligned}
P_{\text{out}}^{\mathrm{I}} &= \begin{cases} \Pr\left\{ y < \frac{\gamma_{\text{th}}\sigma_d^2(1+\kappa g_r)}{\kappa p_s \theta_1\theta_2(1-\kappa\gamma_{\text{th}} g_r)} \right\}, & g_r < \frac{1}{\kappa\gamma_{\text{th}}} \\ 1, & g_r \geq \frac{1}{\kappa\gamma_{\text{th}}} \end{cases} \\
&= \begin{cases} F_y\left(\frac{\gamma_{\text{th}}\sigma_d^2(1+\kappa g_r)}{\kappa p_s \theta_1\theta_2(1-\kappa\gamma_{\text{th}} g_r)} \right), & 0 < \alpha < \frac{1}{1+\eta g_r \gamma_{\text{th}}} \\ 1, & \frac{1}{1+\eta g_r \gamma_{\text{th}}} \leq \alpha < 1 \end{cases} \\
&= \begin{cases} \frac{2^{2-m_1-m_2}}{\Gamma(m_1)\Gamma(m_2)} D_{\mu,\nu}(2\sqrt{\xi}), & 0 < \alpha < \frac{1}{1+\eta g_r \gamma_{\text{th}}} \\ 1, & \frac{1}{1+\eta g_r \gamma_{\text{th}}} \leq \alpha < 1, \end{cases}
\end{aligned}
\tag{A.6}
$$

where $\xi \triangleq \frac{\gamma_{\text{th}}\sigma_d^2(1+\kappa g_r)}{\kappa p_s \theta_1\theta_2(1-\kappa\gamma_{\text{th}} g_r)}$. By substituting (A.2), (A.3), and (A.6) into $P_{\text{out}} = \Pr\left\{ g_1 < \frac{S_{\min}}{p_s} \right\} + \Pr\left\{ g_1 \geq \frac{S_{\min}}{p_s} \right\} P_{\text{out}}^{\mathrm{I}}$, we arrive at (15).

Appendix B: A proof of Proposition 2

From (A.6), we know that $P_{\text{out}}^{\mathrm{I}} = 1$ when $\alpha \in \left[\frac{1}{1+\eta g_r \gamma_{\text{th}}}, 1 \right)$. When $\alpha \in \left(0, \frac{1}{1+\eta g_r \gamma_{\text{th}}} \right)$, $P_{\text{out}}^{\mathrm{I}} = F_y(2\sqrt{\xi})$, which is a non-decreasing CDF of y with respect to $2\sqrt{\xi}$, where ξ is given by (17). Thus, minimizing $P_{\text{out}}^{\mathrm{I}}$ is equivalent to minimizing ξ with respect to $\alpha \in \left(0, \frac{1}{1+\eta g_r \gamma_{\text{th}}} \right)$. Since there exists a one-to-one mapping from $\alpha \in (0,1)$ to $\kappa \in (0,\infty)$, minimizing ξ with respect to $\alpha \in \left(0, \frac{1}{1+\eta g_r \gamma_{\text{th}}} \right)$ is equivalent to minimizing ξ with respect to $\kappa \in \left(0, \frac{1}{g_r \gamma_{\text{th}}} \right)$.

The second order derivative of ξ with respect to κ can be expressed as

$$
\frac{\partial^2 \xi}{\partial \kappa^2} = -\frac{2\gamma_{\text{th}}\sigma_d^2(1 - 3g_r\kappa\gamma_{\text{th}} + 3g_r^2\kappa^2\gamma_{\text{th}}^2 + g_r^3\kappa^3\gamma_{\text{th}}^2)}{\kappa^3 p_s\theta_1\theta_2(-1+g_r\kappa\gamma_{\text{th}})^3}. \tag{B.1}
$$

Based on the fact that $\kappa \in \left(0, \frac{1}{g_r\gamma_{\text{th}}} \right)$, we have $-1+g_r\kappa\gamma_{\text{th}} < 0$ and $1 - 3g_r\kappa\gamma_{\text{th}} + 3g_r^2\kappa^2\gamma_{\text{th}}^2 + g_r^3\kappa^3\gamma_{\text{th}}^2 > 0$. Thus, it can be shown that $\frac{\partial^2\xi}{\partial\kappa^2} > 0$ and ξ is a convex function of $\kappa \in \left(0, \frac{1}{g_r\gamma_{\text{th}}} \right)$. By solving $\frac{\partial\xi}{\partial\kappa} = 0$ with respect to κ, the achievable minimum ξ is obtained by

$$
\bar{\kappa} = \frac{1}{g_r\gamma_{\text{th}}} \left(\sqrt{\gamma_{\text{th}}(\gamma_{\text{th}}+1)} - \gamma_{\text{th}} \right). \tag{B.2}
$$

Then, by substituting (B.2) into $\bar{\alpha} = \frac{\bar{\kappa}}{\eta+\bar{\kappa}}$, we have

$$
\bar{\alpha} = \frac{1}{1+\eta g_r(\sqrt{\gamma_{\text{th}}(\gamma_{\text{th}}+1)} + \gamma_{\text{th}})}, \tag{B.3}
$$

which is the TS factor that achieves the minimum information outage probability. Due to the uniqueness of $\bar{\alpha}$, it is also the TS factor that achieves the allowable maximum average throughput. By substituting (B.3) into (16), the achieved minimum information outage probability can be expressed as

$$
\bar{P}_{\text{out}}^{\mathrm{I}} = \frac{2^{2-m_1-m_2}}{\Gamma(m_1)\Gamma(m_2)} D_{\mu,\nu}\left(2\sqrt{\bar{\xi}} \right), \tag{B.4}
$$

where

$$
\bar{\xi} \triangleq \frac{g_r\gamma_{\text{th}}\sigma_d^2\left(2\left(\gamma_{\text{th}} + \sqrt{\gamma_{\text{th}}(\gamma_{\text{th}}+1)} \right) + 1 \right)}{p_s\theta_1\theta_2}. \tag{B.5}
$$

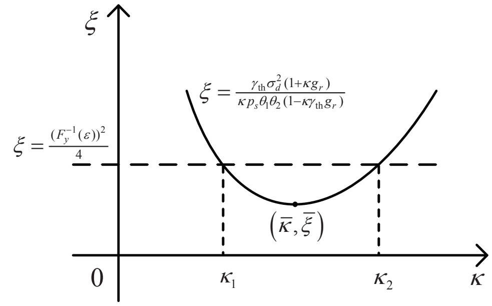

Fig. C.1. An illustration of ξ versus κ.

Appendix C: A proof of Proposition 3

Following the procedures at the beginning of Appendix B, we choose to optimize $\kappa \in \left(0, \frac{1}{g_r\gamma_{\text{th}}} \right)$ with its one-to-one mapping to $\alpha \in \left(0, \frac{1}{1+\eta g_r\gamma_{\text{th}}} \right)$ to maximize the average throughput subject to Q_2. Based on the results from (B.1) to (B.5), we know that $\xi = \frac{\gamma_{\text{th}}\sigma_d^2(1+\kappa g_r)}{\kappa p_s\theta_1\theta_2(1-\kappa\gamma_{\text{th}}g_r)}$ is a convex function of $\kappa \in \left(0, \frac{1}{g_r\gamma_{\text{th}}} \right)$ and the achievable minimum ξ is given by (B.5). Note that $Q_2 := \{ P_{\text{out}}^{\mathrm{I}} = F_y(2\sqrt{\xi}) \leq \varepsilon \}$ can be rewritten as $Q_2 := \left\{ \xi \leq \frac{(F_y^{-1}(\varepsilon))^2}{4} \right\}$, which can be satisfied only when $\bar{\xi} \leq \frac{(F_y^{-1}(\varepsilon))^2}{4}$, i.e., $g_r \leq \hat{g}_r$, where

$$
\hat{g}_r \triangleq \frac{p_s\theta_1\theta_2(F_y^{-1}(\varepsilon))^2}{4\gamma_{\text{th}}\sigma_d^2\left(2\left(\gamma_{\text{th}} + \sqrt{\gamma_{\text{th}}(\gamma_{\text{th}}+1)} \right) + 1 \right)}. \tag{C.1}
$$

Moreover, when $g_r > \hat{g}_r$, we have $\bar{\xi} > \frac{(F_y^{-1}(\varepsilon))^2}{4}$, so that Q_2 cannot be satisfied.

As illustrated in Fig. C.1, when $g_r \leq \hat{g}_r$, there are two cross-over points κ_1 and κ_2 between $\xi = \frac{(F_y^{-1}(\varepsilon))^2}{4}$ and $\xi = \frac{\gamma_{\text{th}}\sigma_d^2(1+\kappa g_r)}{\kappa p_s\theta_1\theta_2(1-\kappa\gamma_{\text{th}}g_r)}$ due to the convexity of $\xi = \frac{\gamma_{\text{th}}\sigma_d^2(1+\kappa g_r)}{\kappa p_s\theta_1\theta_2(1-\kappa\gamma_{\text{th}}g_r)}$ with respect to κ. Without loss of generality, we choose $\kappa_1 \leq \kappa_2$, where the equality holds when $g_r = \hat{g}_r$, so that the QoS constraint Q_2 is satisfied by $\kappa \in [\kappa_1, \kappa_2]$. When the target information outage probability can be achieved, the average throughput can be approximated as [27]

$$
\hat{R}_{\text{HT}} = (1-\alpha)(1-\varepsilon)\bar{F}_{g_1}\left(\frac{S_{\min}}{p_s} \right) R. \tag{C.2}
$$

The above average throughput is maximized with the allowable minimum α (or equivalently the allowable minimum κ) that satisfies Q_2. Thus, the average throughput is maximized by $\hat{\kappa}$ of (27), which is obtained as $\hat{\kappa} = \kappa_1$ by solving $\xi = \frac{\gamma_{\text{th}}\sigma_d^2(1+\kappa g_r)}{\kappa p_s\theta_1\theta_2(1-\kappa\gamma_{\text{th}}g_r)} = \frac{(F_y^{-1}(\varepsilon))^2}{4}$. Then, the TS factor that maximizes the average throughput subject to Q_2 can be expressed as

$$
\hat{\alpha} = \begin{cases} \frac{\hat{\kappa}}{\eta+\hat{\kappa}}, & g_r \leq \hat{g}_r \\ \text{does not exsit}, & \text{otherwise}. \end{cases} \tag{C.3}
$$

References

[1] X. Zhou, R. Zhang, and C. K. Ho, “Wireless information and power transfer: Architecture design and rate-energy tradeoff,” *IEEE Trans. Commun.*, vol. 61, no. 11, pp. 4754–4767, Nov. 2013.

[2] H. Tabassum, E. Hossain, A. Ogundipe, and D. I. Kim, “Wireless-powered cellular networks: key challenges and solution techniques,” *IEEE Commun. Mag.*, vol. 53, no. 6, pp. 63–71, Jun. 2015.

[3] I. Krikidis, S. Timotheou, S. Nikolaou, G. Zheng, D. Ng, and R. Schober, "Simultaneous wireless information and power transfer in modern communication systems," *IEEE Commun. Mag., Green Communications and Computing Networks Series*, vol. 52, no. 11, pp. 104–110, Nov. 2014.
[4] A. Nasir, X. Zhou, S. Durrani, and R. Kennedy, "Relaying protocols for wireless energy harvesting and information processing," *IEEE Trans. Wireless Commun.*, vol. 12, no. 7, pp. 3622–3636, Jul. 2013.
[5] ——, "Throughput and ergodic capacity of wireless energy harvesting based DF relaying network," in *Proc. IEEE ICC 2014*, Sydney, Australia, 10-14 Jun. 2014, pp. 4066–4071.
[6] Z. Ding, S. M. Perlaza, I. Esnaola, and H. V. Poor, "Power allocation strategies in energy harvesting wireless cooperative networks," *IEEE Trans. Wireless Commun.*, vol. 13, no. 2, pp. 846–860, Feb. 2014.
[7] I. Krikidis, S. Sasaki, S. Timotheou, and Z. Ding, "A low complexity antenna switching for joint wireless information and energy transfer in MIMO relay channels," *IEEE Trans. Commun.*, vol. 62, no. 5, pp. 1577–1587, May 2014.
[8] Z. Zhou, M. Peng, Z. Zhao, and Y. Li, "Joint power splitting and antenna selection in energy harvesting relay channels," *IEEE Trans. Signal Process.*, vol. 22, no. 7, pp. 823–827, Jul. 2015.
[9] Z. Ding, C. Zhong, D. W. K. Ng, M. Peng, H. A. Suraweera, R. Schober, and H. V. Poor, "Application of smart antenna technologies in simultaneous wireless information and power transfer," *IEEE Commun. Mag.*, vol. 53, no. 4, Apr. 2015.
[10] Z. Ding, I. Krikidis, B. Sharif, and H. V. Poor, "Wireless information and power transfer in cooperative networks with spatially random relays," *IEEE Trans. Wireless Commun.*, vol. 13, no. 8, pp. 4440–4453, Aug. 2014.
[11] H. Chen, Y. Li, Y. Jiang, Y. Ma, and B. Vucetic, "Distributed power splitting for SWIPT in relay interference channels using game theory," *IEEE Trans. Wireless Commun.*, vol. 14, no. 1, pp. 410–420, Aug. 2014.
[12] A. Sabharwal, P. Schniter, D. Guo, D. Bliss, S. Rangarajan, and R. Wichman, "In-band full-duplex wireless: Challenges and opportunities," *IEEE J. Sel. Areas in Commun.*, vol. 32, no. 9, pp. 1637–1652, Sept. 2014.
[13] T. Riihonen, S. Werner, and R. Wichman, "Hybrid full-duplex/half-duplex relaying with transmit power adaptation," *IEEE Trans. Wireless Commun.*, vol. 10, no. 9, pp. 3074–3085, Sept. 2011.
[14] C. Zhong, H. Suraweera, G. Zheng, I. Krikidis, and Z. Zhang, "Wireless information and power transfer with full duplex relaying," *IEEE Trans. Commun.*, vol. 62, no. 10, pp. 3447–3461, Oct. 2014.
[15] C. Zhong, H. A. Suraweera, G. Zheng, I. Krikidis, and Z. Zhang, "Improving the throughput of wireless powered dual-hop systems with full duplex relaying," in *Proc. IEEE ICC 2015*, London, UK, 8-12 Jun. 2015, pp. 4253–4258.
[16] G. Liu, H. Ji, F. Yu, Y. Li, and R. Xie, "Energy-efficient resource allocation in full-duplex relaying networks," in *Proc. IEEE ICC 2014*, Sydney, Australia, 10-14 Jun. 2014, pp. 2400–2405.
[17] H. Kim, S. Lim, H. Wang, and D. Hong, "Optimal power allocation and outage analysis for cognitive full duplex relay systems," *IEEE Trans. Wireless Commun.*, vol. 11, no. 10, pp. 3754–3765, Oct. 2012.
[18] H. Ju, S. Lim, D. Kim, D. Hong, and H. V. Poor, "Full duplexity in beamforming-based multi-hop relay networks," *IEEE J. Sel. Areas in Commun.*, vol. 30, no. 8, pp. 1554–1565, Sept. 2012.
[19] M. Mohammadi, H. Suraweera, G. Zheng, C. Zhong, and I. Krikidis, "Full-duplex MIMO relaying powered by wireless energy transfer," in *Proc. 16th SPAWC*, Stockholm, Sweden, 28 Jun.-1 July 2015, pp. 296–300.
[20] Y. Zeng and R. Zhang, "Full-duplex wireless-powered relay with self-energy recycling," *IEEE Wireless Commun. Lett.*, vol. 4, no. 2, pp. 201–204, Feb. 2015.
[21] Q. Shi, L. Liu, W. Xu, and R. Zhang, "Joint transmit beamforming and receive power splitting for MISO SWIPT systems," *IEEE Trans. Wireless Commun.*, vol. 13, no. 6, pp. 3269–3280, Jun. 2014.
[22] S. Timotheou, I. Krikidis, G. Zheng, and B. Ottersten, "Beamforming for MISO interference channels with QoS and RF energy transfer," *IEEE Trans. Wireless Commun.*, vol. 13, no. 5, pp. 2646–2658, May 2014.
[23] Y. Dong, M. J. Hossain, and J. Cheng, "Joint power control and time switching for SWIPT systems with heterogeneous QoS requirements," *IEEE Commun. Letters*, vol. 20, no. 2, pp. 328–331, Feb. 2016.
[24] A. Dong, H. Zhang, D. Wu, and D. Yuan, "QoS-constrained transceiver design and power splitting for downlink multiuser MIMO SWIPT systems," in *Proc. IEEE ICC 2016*, London, UK, 22-27, May 2016, pp. 1–6.
[25] H. Chen, Y. Ma, Z. Lin, Y. Li, and B. Vucetic, "Distributed power control in interference channels with QoS constraints and RF energy harvesting: A game-theoretic approach," *IEEE Trans. Veh. Technol.*, vol. PP, no. 99, pp. 1–7, Mar. 2016.
[26] Y. Zeng and R. Zhang, "Optimized training design for wireless energy transfer," *IEEE Trans. Commun.*, vol. 63, no. 2, pp. 536–550, Feb. 2015.
[27] P. Wu and N. Jindal, "Performance of hybrid-ARQ in block-fading channels: A fixed outage probability analysis," *IEEE Trans. Commun.*, vol. 58, no. 4, pp. 1129–1141, Apr. 2010.
[28] Y. Dong, M. J. Hossain, and J. Cheng, "Performance of wireless powered amplify and forward relaying over Nakagami-m fading channels with nonlinear energy harvester," *IEEE Commun. Letters*, vol. 20, no. 4, pp. 672–675, Apr. 2016.
[29] M. Duarte, C. Dick, and A. Sabharwal, "Experiment-driven characterization of full-duplex wireless systems," *IEEE Trans. Wireless Commun.*, vol. 11, no. 12, pp. 4296–4307, Dec. 2012.
[30] N. Tran, L. Rodriguez, and T. Le-Ngoc, "Optimal power control and error performance for full-duplex dual-hop AF relaying under residual self-interference," *IEEE Commun. Letters*, vol. 19, no. 2, pp. 291–294, Feb. 2015.
[31] L. Jimenez Rodriguez, N. Tran, and T. Le-Ngoc, "Performance of full-duplex AF relaying in the presence of residual self-interference," *IEEE J. Sel. Areas in Commun.*, vol. 32, no. 9, pp. 1752–1764, Sept. 2014.
[32] I. Krikidis, S. Timotheou, and S. Sasaki, "RF energy transfer for cooperative networks: Data relaying or energy harvesting?" *IEEE Commun. Letters*, vol. 16, no. 11, pp. 1772–1775, Nov. 2012.
[33] I. Krikidis, "Relay selection in wireless powered cooperative networks with energy storage," *IEEE J. Sel. Areas in Commun.*, vol. 33, no. 12, pp. 2596–2610, Dec. 2015.
[34] I. S. Gradshteyn and I. M. Ryzhik, *Table of Integrals, Series, and Products*. New York: Academic Press, 2007.
[35] D. Korpi, T. Riihonen, V. Syrjala, L. Anttila, M. Valkama, and R. Wichman, "Full-duplex transceiver system calculations: Analysis of ADC and linearity challenges," *IEEE Trans. Wireless Commun.*, vol. 13, no. 7, pp. 3821–3836, Jul. 2014.
[36] A. Masmoudi and T. Le-Ngoc, "Residual self-interference after cancellation in full-duplex systems," in *Proc. 2014 IEEE ICC*, Sydney, Australia, 10-14 Jun. 2014, pp. 4680–4685.
[37] M. Stoopman, S. Keyrouz, H. J. Visser, K. Philips, and W. A. Serdijn, "Co-design of a CMOS rectifier and small loop antenna for highly sensitive RF energy harvesters," *IEEE J. Solid-State Circuits*, vol. 49, no. 3, pp. 622–634, Mar. 2014.
[38] A. Chuang, A. G. i Fabregas, L. K. Rasmussen, and I. B. Collings, "Optimal throughput-diversity-delay tradeoff in MIMO ARQ block-fading channels," *IEEE Trans. Inf. Theory*, vol. 54, no. 9, pp. 3968–3986, Sept. 2008.
[39] A. Lozano and N. Jindal, "Transmit diversity vs. spatial multiplexing in modern MIMO systems," *IEEE Trans. Wireless Commun.*, vol. 9, no. 1, pp. 186–197, Jan. 2010.
[40] H. A. Suraweera, P. J. Smith, A. Nallanathan, and J. S. Thompson, "Amplify-and-forward relaying with optimal and suboptimal antenna selection," *IEEE Trans. Wireless Commun.*, vol. 10, pp. 1874–1885, Jun. 2011.
[41] W. J. Huang, Y. W. P. Hong, and C. C. J. Kuo, "Lifetime maximization for amplify-and-forward cooperative networks," *IEEE Trans. Wireless Commun.*, vol. 7, no. 5, pp. 1800–1805, May 2008.
[42] I. Krikidis, T. Charalambous, and J. S. Thompson, "Buffer-aided relay selection for cooperative diversity systems without delay constraints," *IEEE Trans. Wireless Commun.*, vol. 11, no. 5, pp. 1957–1967, May 2012.
[43] C. S. Withers and S. Nadarajah, "On the product of gamma random variables," *Quality & Quantity*, vol. 47, no. 1, pp. 545–552, Mar. 2011.

Hongwu Liu received the Ph.D. degree from Southwest Jiaotong University in 2008. From 2008 to 2010, he was with Nanchang Hangkong University. From 2010 to 2011, he was a Post-Doctoral Fellow with the Shanghai Institute of Microsystem and Information Technology, Chinese Academy of Science. From 2011 to 2013, he was a Research Fellow with the UWB Wireless Communications Research Center, Inha University, South Korea. He is currently an Associate Professor with Shandong Jiaotong University. His current research interests include MIMO signal processing, cognitive radios, cooperative communications, wireless secrecy communications, and future Internet of Things.

Kyeong Jin Kim (SM'11) received the M.S. degree from Korea Advanced Institute of Science and Technology, Daejeon, South Korea, in 1991, and the M.S. and Ph.D. degrees in electrical and computer engineering from the University of California, Santa Barbara, CA, USA in 2000. From 1991 to 1995, he was a Research Engineer with the Video Research Center of Daewoo Electronics, Ltd., South Korea. In 1997, he joined the Data Transmission and Networking Laboratory, University of California at Santa Barbara. After receiving his degrees, he joined the Nokia research center and Nokia Inc., Dallas, TX, USA, as a Senior Research Engineer, where he was an L1 specialist, from 2005 to 2009. From 2010 to 2011, he was an Invited Professor with Inha University, Incheon, South Korea. Since 2012, he has been working as a Senior Principal Research Scientist with the Mitsubishi Electric Research Laboratories, Cambridge, MA. His current research interests include transceiver design, resource management, scheduling in the cooperative wireless communications systems, cooperative spectrum sharing system, physical layer secrecy system, and device-to-device communications.

Dr. Kim currently serves as an Editor of the IEEE TRANSACTIONS ON COMMUNICATIONS. He served as an Editor of the IEEE COMMUNICATIONS LETTERS and INTERNATIONAL JOURNAL OF ANTENNAS AND PROPAGATION. He also served as a Guest Editor of the EURASIP JOURNAL ON WIRELESS COMMUNICATIONS AND NETWORKING Special Issue on Cooperative Cognitive Networks and IET COMMUNICATIONS Special Issue on Secure Physical Layer Communications.

Kyung Sup Kwak received the Ph.D. degree from the University of California at San Diego. He worked for Hughes Network Systems, and IBM Network Analysis Center, USA. Since then he has been with the School of Information and Communication Engineering, Inha University, South Korea, as a professor, and served the dean of the Graduate School of Information Technology and Telecommunications and the director of UWB Wireless Communications Research Center, an IT research center, South Korea, since 2003. In 2006, he served as the President of Korean Institute of Communication Sciences (KICS), and in 2009, the President of Korea Institute of Intelligent Transport Systems. He has authored or co-authored over 200 peer-reviewed journal papers and served as TPC and Track chairs/organizing chairs for several IEEE related conferences. His current research interests include multiple access communication systems, mobile and UWB radio systems, future Internet of Things, and wireless body area network: nano network and Molecular Communications. In 1993, he received the Engineering College Achievement Award from Inha University and the Service Award from the Institute of Electronics Engineers of Korea, in 1996 and 1999, respectively, and distinguished service awards from the KICS. He received the LG Paper Award in 1998 and the Motorola Paper Award in 2000. He received official commendations for UWB radio technology research and development from Minister of Information and Communication, Prime Minister, and President of Korea, in 2005, 2006, and 2009. In 2007, he received the Haedong Paper Award and in 2009, the Haedong Scientific Award of research achievement. In 2008, he was elected an Inha Fellow Professor and he is currently an Inha Hanlim Fellow Professor.

H. Vincent Poor (S72-M77-SM82-F87) received the Ph.D. degree in EECS from Princeton University in 1977. From 1977 until 1990, he was on the faculty of the University of Illinois at Urbana-Champaign. Since 1990, he has been on the faculty at Princeton, where he is currently the Michael Henry Strater University Professor of Electrical Engineering. From 2006 to 2016, he served as the Dean of Princeton's School of Engineering and Applied Science. His research interests are in the areas of information theory, statistical signal processing and stochastic analysis, and their applications in wireless networks and related fields such as smart grid and social networks. Among his publications in these areas is the book *Mechanisms and Games for Dynamic Spectrum Allocation* (Cambridge University Press, 2014).

Dr. Poor is a member of the National Academy of Engineering and the National Academy of Sciences, and is a foreign member of the Royal Society. He is also a fellow of the American Academy of Arts and Sciences, the National Academy of Inventors, and other national and international academies. He received the Marconi and Armstrong Awards of the IEEE Communications Society in 2007 and 2009, respectively. Recent recognition of his work includes the 2016 John Fritz Medal, the 2017 IEEE Alexander Graham Bell Medal, Honorary Professorships at Peking University and Tsinghua University, conferred in 2016, and a Doctor of Science *honoris causa* from Syracuse University in 2017.